Mon. Not. R. Astron. Soc. **000**, 1–?? (2024) Printed 26 December 2024 (MN LATEX style file v2.2)

An MHD-based model for wind-driven disc-planet interactions

Michael Hammer[1⋆], Min-Kai Lin[1,2]
[1] *Institute of Astronomy and Astrophysics, Academia Sinica, Taipei 10617, Taiwan*
[2] *Physics Division, National Center for Theoretical Sciences, Taipei 10617, Taiwan*

Accepted XXX. Received YYY; in original form ZZZ

ABSTRACT
Hydrodynamic simulations of protoplanetary discs with planets typically assume that the disc is viscously driven, even though magnetic disc winds are now considered the primary driver of angular momentum transport through the disc. Magnetic disc winds are typically left out of hydrodynamic simulations because they require a magneto-hydrodynamic (MHD) treatment and an entire 3D domain, both of which are computationally expensive. Some studies have attempted to incorporate disc winds into disc-planet simulations without full MHD by adding a torque to mimic the effects of a disc wind. However, these studies predate any explicit 3D MHD simulations of planets in the presence of a disc wind. In light of recent MHD studies of disc winds beginning to include a planet, we develop a new disc wind prescription based on these studies and test its efficacy. With three main components, namely (i) excess torque in the planetary gap region, (ii) an MHD-based radial profile for the background torque, and (iii) a moderate level of viscosity, we find that we can essentially reproduce planetary gap profiles for planets above the thermal mass. With lower-mass planets, however, we find it more difficult to reproduce their gap structure. Lastly, we explore the planet's migration path and find that the planet rapidly migrates inwards due to the excess torque in the gap.

Key words: transition discs – instability, hydrodynamics, methods:numerical, protoplanetary discs

1 INTRODUCTION

The hallmark feature of protoplanetary discs in ALMA observations of mm dust is an alternating pattern of gaps and rings spread across the disc (e.g. Andrews et al. 2018). It is preferentially expected that planets are responsible for carving out many of these gaps, expelling material away from their vicinity as they orbit. Whether a planet is massive enough to open up a gap depends on whether its gravitational torque can compete against the torques associated with the flow of angular momentum transport through the disc. As a result, it is critical for hydrodynamic simulations to accurately represent the flow of angular momentum transport to infer planet and disc properties from observations or to model the planet's orbital migration.

How do protoplanetary discs transport angular momentum? They do not have an appreciable molecular viscosity. Nevertheless, they must be capable of transporting or losing angular momentum to explain observed stellar accretion rates (e.g. Alexander et al. 2014; Hartmann et al. 2016). It was long accepted that a turbulent viscosity arising from magneto-hydrodynamic (MHD) effects, namely the magneto-rotational instability (MRI: Balbus & Hawley 1998), was responsible. However, MHD studies have recently demonstrated that non-ideal MHD effects suppress the MRI (Bai & Stone 2013; Bai 2017), particularly in the disc's midplane. The suppression of the MRI gives way for other MHD effects, particularly laminar magnetic stresses and magnetically driven disc winds (Bai & Stone 2013; Bai et al. 2016), to transport or remove angular momentum, respectively.

Magnetic winds refer to the magnetically-driven ejection of material from the surface of the disc. The ejected material gets caught along poloidal magnetic field lines and is expelled outwards due to the rotation of the disc (Blandford & Payne 1982). The magnetic field lines responsible thread the midplane and extend to large distances both radially and vertically away from the launching point. The outwards ejection of material and removal of angular momentum gives rise to a corresponding inward flow of material, often primarily near the surface of the disc.

The large radial and vertical extents of the magnetic field lines that govern disc winds require simulations of this phenomenon to have large computational domains in the radial and latitudinal directions, in addition to full MHD as well as the relevant non-ideal MHD effects one would want to include to make the study applicable to protoplanetary discs. Studies that include a planet also require 3D. As a result, 3D MHD studies of planetary gap profiles in wind-driven discs only began very recently (Aoyama & Bai 2023; Wafflard-Fernandez & Lesur 2023; Hu et al. 2025). Each study, however, only covered a small number of cases over a limited number of orbits. Due to the high computational cost of explicit 3D MHD simulations, it would be advantageous if disc winds could be modeled within a 2D hydrodynamic framework, as is already ubiq-

⋆ E-mail: mhammer@arizona.edu

uitously done with the α-viscosity prescription (Shakura & Sunyaev 1973) for viscous discs. This would make it possible to run larger parameter studies and much longer simulations than are currently feasible with 3D MHD.

Indeed, even before 3D MHD studies were carried out, several recent works attempted to model disc-planet interactions with disc winds without explicit MHD, mainly to study planet migration in 2D (Kimmig et al. 2020) and 3D (Lega et al. 2022), to study gap profiles (Elbakyan et al. 2022), or planet-induced vortices (Wu et al. 2023). These works incorporated disc winds by prescribing the torque due to the wind, and may also include a mass loss term corresponding to the wind. Kimmig et al. (2020) and Lega et al. (2022) found that disc winds altered the co-rotation region enough for planets to unusually migrate outwards. Elbakyan et al. (2022) and Wu et al. (2023) found very different gap profiles compared to wind-less discs in which the outer gap edge ended up much closer to the planet.

It remained unclear whether those models and results would hold up against explicit MHD simulations. With such simulations now available, it is of interest to improve hydrodynamic prescriptions of disc winds so they could be used for long-term simulations and parameter studies that are still not that feasible with explicit MHD. All three of Aoyama & Bai (2023); Wafflard-Fernandez & Lesur (2023); Hu et al. (2025) found that wind produces a much stronger torque in the gap, which carves out a deeper at a much faster rate. The outer gap edge was also not noticeably closer to the planet like with prescribed models. Lastly, Aoyama & Bai (2023) found the expected planet migration direction to be inwards, even though the co-rotation region was disrupted in a similar manner to what can happen with a prescribed model.

Aoyama & Bai (2023) did attempt to fit their 3D MHD gap profiles with 2D hydrodynamics, albeit only with viscous and inviscid models, not any prescribed wind models. They recommended their inviscid model as the better way to mimic 3D MHD. Nonetheless, they did not find either model to be adequate, motivating the need for a prescribed wind model to produce a more optimal fit.

In this work, we design a new disc wind prescription model and test if it can better match the gap profiles from the MHD simulations with disc winds, focusing on the study by Aoyama & Bai (2023), hereafter A&B 2023, for comparison. We use Kimmig et al. (2020), hereafter K20, as a reference wind model to test if and how our model makes a difference. We also use our wind model to explore how the planet migrates in these conditions.

This paper is organized as follows: In Section 2, we describe the setup for our 2D simulations, including the components of our disc wind model and their motivation. We also review the reference prescribed model. In Section 3, we calibrate our prescribed wind model, component-to-component, by matching the resulting gap profile with that found in explicit MHD simulations. We review each component's role and demonstrate that changing the parameter values does not improve the model. In Section **??**, we apply our new prescription model to study the windy disk-planet interaction in scenarios not yet explored by explicit MHD simulations, while keeping the planet on a fixed orbit. In Section 5, we apply the model to a migrating planet, exploring cases both with inwards and outwards migration expected. In Section 6, we discuss the validity of our model and how it could be applied to other studies. In Section 7, we conclude our results.

2 SETUP

We consider a 2D viscous disc of gas and dust harbouring a planet in orbit around a star of mass $M_\star$ at the center of the system. The gas is subject to the effects of a disc wind, namely an inward torque driven by the wind and mass lost to the wind.

2.1 Disc model

The disc is set in a cylindrical polar coordinate system (r, ϕ, z) centered at the star. With the disc's thin structure, we assume the razor thin disc approximation and treat the disc as 2D, where the 2D state variables are vertical averages of their 3D counterparts. The disc's evolution in time t is dictated by the Navier-Stokes equations, specifically the continuity equation and the momentum equation. The gas continuity equation governing the evolution of the surface density Σ is

$$\frac{\partial \Sigma}{\partial t} + \vec{\nabla} \cdot (\Sigma \vec{v}) = -\dot{\Sigma}_{\rm wind}, \tag{1}$$

where $\vec{v}$ is the velocity vector and $\dot{\Sigma}_{\rm wind}$ is the mass loss term due to the wind. The momentum equation governing the velocity is

$$\begin{aligned}\Sigma\Big(\frac{\partial \vec{v}}{\partial t} + \vec{v} \cdot \vec{\nabla}\vec{v}\Big) = &- \vec{\nabla}P - \Sigma\vec{\nabla}\Phi + \vec{\nabla} \cdot \overleftrightarrow{T} - f_{\rm wind}\hat{\phi} \\ &- \Sigma[2\vec{\Omega}_{\rm f} \times \vec{v} + \vec{\Omega}_{\rm f} \times \big(\vec{\Omega}_{\rm f} \times \vec{r}\big) + \dot{\vec{\Omega}}_{\rm f} \times \vec{r}]\end{aligned} \tag{2}$$

where P is the pressure, Φ is the gravitational potential, $\vec{\Omega}_{\rm f}$ is the angular frequency vector of the reference frame, $f_{\rm wind}$ is the force due to the torque from the wind, and $\mathcal{T}$ is the stress tensor. The gravitational potential Φ is the sum of the star's potential $\Phi_\star$, the planet's potential $\Phi_{\rm p}$, and the indirect potential $\Phi_{\rm i}$ arising from the non-inertial reference frame. The stress tensor is given by

$$\overleftrightarrow{\mathcal{T}} = \Sigma\nu\Big[\vec{v} + (\vec{v})^T - \frac{2}{3}(\vec{\nabla} \cdot \vec{v})\vec{I}\Big], \tag{3}$$

where ν is the kinematic viscosity of the disk and $\vec{I}$ is the identity tensor. The disc is assumed to be locally isothermal, neglecting the energy equation, to match the MHD simulations with disc winds that we wish to compare to. As such, the pressure relates to the density as $P = \Sigma c_{\rm s}^2$, where $c_{\rm s} = H\Omega$ is the sound speed, H is the disc scale height, and Ω is the orbital frequency. The disc aspect ratio is kept flat – in other words, with no flaring – such that $h = H/r$. The orbital frequency is the Keplerian orbital frequency $\Omega \approx \Omega_{\rm K} = \sqrt{GM_\star/r^3}$, where G is the gravitational constant. As such, the sound speed scales as $c_{\rm s} \propto r^{-1/2}$. Our fiducial setup uses a constant ν throughout the disc, but some alternate setups use the standard α-viscosity model (Shakura & Sunyaev 1973), where $\nu = \alpha c_{\rm s} H$.

The dust is small enough to be treated as a fluid. It behaves according to the same equations as the gas, except that it is affected by drag forces between the gas and the dust instead of pressure or viscosity. The additional drag force terms in the momentum equation are:

$$\left.\frac{\partial v_{\rm r,d}}{\partial t}\right|_{\rm drag} = -\frac{v_{\rm r,d} - v_{\rm r}}{t_{\rm s}}, \tag{4}$$

$$\left.\frac{\partial v_{\phi,\rm d}}{\partial t}\right|_{\rm drag} = -\frac{v_{\phi,\rm d} - v_{\phi}}{t_{\rm s}}, \tag{5}$$

where $v_{\rm r}$ and v_ϕ are the radial and azimuthal velocity components of the gas, and $v_{\rm r,d}$ and $v_{\phi,\rm d}$ are the radial and azimuthal velocity

components of the dust. The stopping time is defined in the midplane as

$$t_{\rm s} = \frac{\rm St}{\Omega} = \left(\frac{\pi}{2}\frac{\rho_{\rm d} s}{\Sigma}\right)\frac{1}{\Omega}, \tag{6}$$

where $\rho_{\rm d} = 1$ g / cm^3 is the physical density of each dust grain, and s is the size of each grain. Because of the small size of the grains near millimeter-size, the stopping time is in the Epstein regime (Weidenschilling 1977). Its dimensionless form is the Stokes number St, and we consider grains with fixed St.

Beyond drag forces, another effect only experienced by the dust is diffusion, which is part of the dust continuity equation and defined as

$$\left.\frac{\partial \Sigma_{\rm d}}{\partial t}\right|_{\rm diff} = \nabla \cdot \left(D \Sigma_{\rm tot} \nabla \left(\frac{\Sigma_{\rm d}}{\Sigma_{\rm tot}}\right)\right), \tag{7}$$

where $\Sigma_{\rm d}$ is the dust surface density, $\Sigma_{\rm tot} = \Sigma + \Sigma_{\rm d}$ is the total surface density, and the diffusion coefficient is $D = \hat{D} r_{\rm p}^2 \Omega_{\rm p}$ with dimensions in terms of the the planet's semi-major axis $r_{\rm p}$ and the planet's orbital timescale $\Omega_{\rm p}$. The dimensionless diffusion is on the order of the dimensionless viscosity, i.e. $\hat{D} \approx \hat{\nu}$, since the dust grains are small enough to satisfy St $\ll$ 1 (Youdin & Lithwick 2007).

2.2 Planet model

We incorporate the planet as a gravitational potential according to

$$\Phi_{\rm p}(\mathbf{r}, t) = -\frac{G M_{\rm p}}{\sqrt{(\mathbf{r} - \mathbf{r_p})^2 + r_{\rm s}^2}}, \tag{8}$$

where $M_{\rm p}$ is the planet's mass, $r_{\rm s} = 0.6H$ is the planet's smoothing length . We also include the indirect potential $\Phi_{\rm i}(\mathbf{r}, t) = -GM_{\rm p}\,[\mathbf{r} \cdot \mathbf{r}_{\rm p}]/r_{\rm p}^3$ arising from the non-inertial reference frame centered on the star. For convenience, we denote the planet-to-star mass ratio as q. The planet's gravitational sphere of influence, and the width of the gap in particular, scale with its Hill radius $r_{\rm H} = r_{\rm p}\,(q/3)^{1/3}$.

2.3 Disc wind models

We model the magnetically-driven disc wind without any explicit magnetic fields by incorporating its two primary effects, a torque that drives inwards accretion and mass loss due to the wind. First, we summarize the behavior of these effects in MHD simulations along with the relevant theoretical background in Section 2.3.1 and then outline the specifics of our implementation in Section 2.3.2. For reference, we compare our model to that developed by K20, which we review in Section 2.3.3.

2.3.1 Background

With MHD in effect, the wind drives accretion through the conservation of angular momentum. The wind ejects gas from a few scale heights above the midplane up and out of the disc, and this outflow in turn exerts a torque on the disc beneath it. Through the balance of the Lorentz force and the Coriolis force, that torque drives accretion.

Where does the accretion take place? The amplitude of the wind-driven accretion at different heights is related to the balance of those forces through

$$\frac{1}{2}\rho \Omega_{\rm K} v_r \approx \frac{B_z}{4\pi}\frac{\partial B_\phi}{\partial z}, \tag{9}$$

where ρ is the 3D gas density, $\Omega_{\rm K}$ is the Keplerian velocity, and B_ϕ and $B_{\rm z}$ are the azimuthal and vertical components of the magnetic field (Wardle 2007; Bai & Stone 2013). As a result, the wind-driven accretion is stronger at heights where there is a strong vertical gradient in B_ϕ, which typically occurs where is a sign flip in the magnetic field. The general vertical accretion profile can vary. It could be spread across a range of heights from the midplane to the wind base (e.g. Figure 9 in Cui & Bai 2021). It may be confined to a relatively thin current layer near the base of the wind if the field lines near the midplane are too straight and the field strength is constant due to non-ideal diffusive effects (e.g. Figures 10 and 11 in Bai & Stone 2013). The accretion can happen on both sides of the midplane, or only above it in either case.

How does the wind-driven accretion compare to radially-driven accretion such as viscosity? The corresponding vertically-integrated accretion rate induced by the wind torque is

$$\dot{M} = \frac{8\pi}{\Omega} r |\mathcal{T}_{z\phi}^{\rm Max}|_{\rm z_b}, \tag{10}$$

where $\mathcal{T}_{z\phi}^{\rm Max}|_{\rm z_b}$ is the vertical component of the Maxwell stress tensor evaluated a the base of the wind $z = z_{\rm b}$. The level of accretion associated with this Maxwell stress is a factor of h^{-1} stronger than the rate associated with a radially-driven stress $\mathcal{T}_{r\phi}$ (whether Reynolds or Maxwell) of the same magnitude. The quantity $r\mathcal{T}_{z\phi}^{\rm Max}$ is the wind torque itself.

Which torques are associated with the wind? The torque derives from the angular momentum flux associated with the wind. A&B 2023 emphasize that this angular momentum flux involves two components, the cumulative wind torque itself $\Gamma_{\rm wind}$ and the angular momentum flux $J_{\rm Max}$ associated with the horizontal Maxwell stress $T_{r\phi}^{\rm Max}$. These vertical and horizontal components are not truly separate, and are both just components of the poloidal Maxwell stress split for the sake of measuring the fluxes. As such, they can be combined into a single MHD angular momentum flux where $J_{\rm MHD} = J_{\rm Max} + \Gamma_{\rm wind}$. The corresponding MHD torque is then just $dJ_{\rm MHD}/dr$.

What is the radial profile of the torque associated with the wind? The profile for the MHD torque $dJ_{\rm MHD}/dr$ in A&B 2023 is piecewise split into two main regions, one part corresponding to the gap and the rest corresponding to the background away from the gap, as illustrated in their Figure 14. The background torque in the outer disc in particular follows a $r^{-1/2}$ profile. Inside the gap region, the torque is amplified by a factor of about five. This increase is due to the lower density in the gap increasing the magnetic flux concentration. The profile in this region is roughly constant, with a magnitude of about $2.3 \times 10^{-3}\, r_{\rm p}^2 \Sigma_{\rm p} v_{\rm p} \Omega_{\rm p}$ regardless of planet mass, where $\Sigma_{\rm p}$ is the initial surface density at the location of the planet and $v_{\rm p}$ is the velocity of the planet. The width of the gap region scales roughly with the Hill radius, and is about 1.5 to 2.0 $r_{\rm H}$. It's less clear what the behavior of the torque in the inner disc should be since a pure MHD-driven gap (e.g. Riols et al. 2020) forms in all cases at what is considered to be a random location.

What is the radial profile of the accretion rate associated with the wind? The background wind-driven accretion rate has a loosely constant profile in A&B 2023, as illustrated in their Figure 9. The precise power law is slightly negative. Because of the gap's excess torque, each case also has a bump in accretion in the gap, which has a decreasing amplitude with increasing planet mass. In the outer part of the disc away from the planet at $r > 1.5\, r_{\rm p}$, the accretion profile begins to change. In their two cases with lower-mass planets, the accretion starts increasing with radius. Meanwhile in the

highest-mass case, it drops off completely before increasing again like the other cases.

What is the radial profile of the mass lost through the wind? The profile for the wind mass loss in A&B 2023 is highly non-uniform, as illustrated in their Figure 9. The expected ratio of the wind mass loss rate to the wind-driven accretion rate is given as

$$\frac{1}{\dot{M}_{\rm acc}}\frac{d\dot{M}_{\rm wind}}{d\ln r} \approx \frac{1}{2}\frac{1}{(r_{\rm A}/r_{\rm wb})^2-1}, \tag{11}$$

where $\lambda \equiv r_{\rm A}/r_{\rm wb} > 1$ is the magnetic lever arm, $r_{\rm A}$ is the Alfvén radius where the local velocity is the Alfvén velocity $v_{\rm A} = B/\sqrt{4\pi\rho}$, and $r_{\rm wb}$ is the location of the base of the wind (Ferreira & Pelletier 1995; Bai et al. 2016). However, this quantity is not useful near the planet. As a result of there being no poloidal field lines in the gap, mass loss only takes place outside of the planetary gap. In both the interior and exterior regions of the disc, the mass loss rate peaks close to the peak in density at the gap edge, indicating a loose dependence on density between the gap edges. In the gap itself, there is instead a small inflow at a much lower magnitude than the adjacent mass loss.

Is there any turbulence in the disc? Although the disc wind primarily induces laminar accretion, the disc can still have a lower level of turbulence through other magnetic effects such as MRI. Turbulence can manifest through the horizontal Reynolds stress $\mathcal{T}_{r\phi}^{\rm Rey}$ and the horizontal Maxwell stress $\mathcal{T}_{r\phi}^{\rm Max}$, which each correspond to a dimensionless $\alpha \equiv \mathcal{T}_{r\phi}/P$ (Shakura & Sunyaev 1973). Figure 7 of A&B 2023 shows that $\alpha^{\rm Max}$ is easily dominant over $\alpha^{\rm Rey}$ by about an order of magnitude in both the gap and outer disc. Both components are much stronger in the gap, and sharply decay in the outer disc but never flatten out.

2.3.2 *New prescribed model*

We sought to develop a disc wind prescription motivated by the underlying physics of disc winds while focusing on reproducing the gap and outer disc profiles obtained from explicit MHD simulations of planets in wind-driven discs. We do not attempt to model the inner disc due to the purely MHD-driven gaps that form there (A&B 2023). Our goal is to derive a simple prescription to study different parameters and longer timescales that MHD simulations have not yet explored.

This model is tailored towards fitting the MHD gap profiles on the short timescales we have. For the longer-term simulations in the application sections with both a static planet (Section 4.3) and a migrating planet (Section 5), we use a different mass loss prescription, since our fiducial mass loss profile is tailored towards short-term simulations only.

2.3.2.1 Torque prescription Following the largely piecewise torque split in A&B 2023, we prescribe the torque with two largely piecewise components, one for the background and one for the gap, and a smoothing between the two components. We express both components of the vertically-integrated azimuthal forcing in the momentum equation with the form

$$f_{\rm wind} = \frac{1}{2\pi r^2\Sigma}\frac{dJ_{\rm MHD}}{dR} \tag{12}$$

We adopt this form based on Equation 14 from A&B 2023.

We set the MHD torque to be a power law based on the torque profiles from A&B 2023 to be

$$\frac{dJ_{\rm MHD}}{dr} = Kb\hat{r}^n\, r_{\rm p}^2\Sigma_{\rm p}v_{\rm p}\Omega_{\rm p}, \tag{13}$$

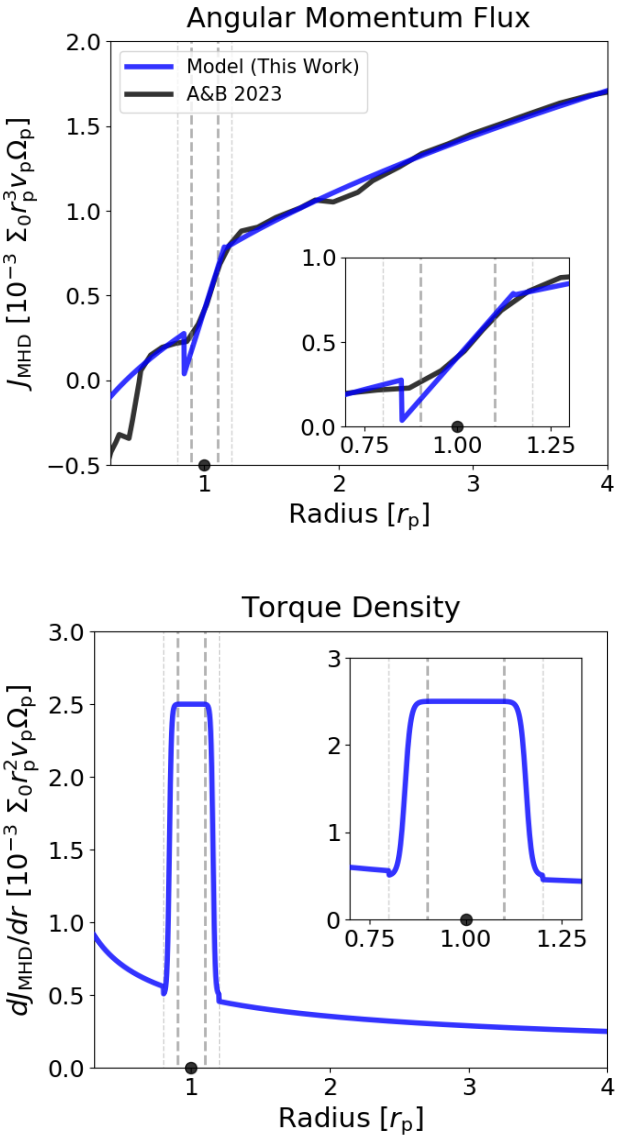

Figure 1. The prescribed torque is based on the angular momentum flux $J_{\rm MHD}$ (*top*) and the resulting torque density $dJ_{\rm MHD}/dr$ (*bottom*). Our prescribed model (*blue*) is intended to match the actual MHD simulation (*black*) by Aoyama & Bai 2023 in the gap and the outer region of the disc. References lines at $\pm 1.0\ r_{\rm H}$ and $\pm 2.0\ r_{\rm H}$ are included (*grey dashed lines*) to help demarcate the different regions, while the planet is indicated with a dot. We include the smoothing of $dJ_{\rm MHD}/dr$ in the plot, which affects the profile mainly at $1.4\ r_{\rm H} \leqslant |r - r_{\rm p}| \leqslant 1.85\ r_{\rm H}$, but leave out the corresponding smoothing of J.

where $\hat{r} = r/r_{\rm p}$, b is the torque coefficient, and both the gap enhancement factor $K(r)$ and the power $n(r)$ vary with radius depending on whether a location is in the gap or not. Specifically, K has the form

$$K(r) = 1 + \frac{1}{2}(K_{\rm gap} - 1)\left[1 - \tanh\left(\frac{\Delta r - r_{\rm t}}{r_{\rm w}}\right)\right], \tag{14}$$

where the smoothing is determined by two parameters: the transition radius $r_{\rm t}$ and the transition width $r_{\rm w}$, while the distance from the planet is $\Delta r \equiv |r - r_{\rm p}|$. Inside the gap, $K \to K_{\rm gap} > 1$, while outside the gap there is no enhancement and $K \to 1$. We set the transition width to be $r_{\rm w} = 0.15\ r_{\rm H}$ and the transition radius

to be $r_{\rm t} = 1.625\ r_{\rm H}$, which is the gap cutoff of $1.5\ r_{\rm H}$ plus half the transition width. (A location outside the gap cutoff is chosen so that the decline in the enhancement factor begins at the edge of the gap, not in it.) On the other hand, the power $n(r)$ is simply defined piecewise as a constant-slope $n = 0$ in the gap and $n = -1/2$ outside the gap. Overall, the full form in the two main regions tends to

$$\frac{dJ_{\rm MHD}}{dr} \rightarrow r_{\rm p}^2 \Sigma_{\rm p} v_{\rm p} \Omega_{\rm p} \begin{cases} K_{\rm gap} b & \text{inside the gap} \\ b\hat{r}^{-1/2} & \text{outside the gap,} \end{cases} \tag{15}$$

where "inside-the-gap" is $\Delta s < 1.5$, "outside-the-gap" is $\Delta s > 2.0$, and the form in the smoothing region ($1.5 < \Delta s < 2.0$) is more complex due to the smoothing of K. We neglected to smooth n because it did not contribute as much to the difference between the magnitude of the torque inside and outside the gap, and would make the model unnecessarily more complicated.

The two physical parameters are set as $b = 5.0 \times 10^{-4}$ and $K_{\rm gap} = 5$ so that $Kb = 2.5 \times 10^{-3}$ in the gap. This gap value is intended to approximately match the value of $dJ_{\rm MHD}/dr \approx 2.3 \times 10^{-3}\ r_{\rm p}^2 \Sigma_{\rm p} v_{\rm p} \Omega_{\rm p}$ that A&B 2023 find in the gap in all cases regardless of planet mass.

The prescribed torque drives mass accretion through the disc. Neglecting the smoothing factor, this accretion rate is

$$\dot{M}(r) = \frac{2}{r\Omega}\frac{dJ_{\rm MHD}}{dr} = 2b\ r_{\rm p}^2 \Sigma_0 \Omega_{\rm p} \begin{cases} K\hat{r}^{-1/2} & \text{inside gap} \\ 1 & \text{outside gap} \end{cases} \tag{16}$$

in the two main regions of the disc. With just this radial dependence of the torque in the model, the accretion would be in a steady state outside of the gap. From inside the gap, there would be excess flow of gas into the inner disc regardless of gap depletion.

The above accretion rate corresponds to an inwards radial velocity of

$$\frac{v_{\rm r}(r)}{v_{\rm p}} = \frac{1}{v_{\rm p}}\frac{2f_{\rm wind}}{\Omega} = \frac{b}{\pi}\frac{1}{\hat{\Sigma}\hat{\Omega}} \begin{cases} K\hat{r}^{-2} & \text{inside the gap} \\ \hat{r}^{-5/2} & \text{outside the gap,} \end{cases} \tag{17}$$

where $\hat{\Sigma} = \Sigma/\Sigma_{\rm p}$ and $\hat{\Omega} = \Omega/\Omega_{\rm p}$. With the surface density power law of $\Sigma \propto r^{-1.25}$ from A&B 2023, this radial velocity has a negative power law everywhere in the disc, but is closer to constant outside the gap at $v_{\rm r} \propto r^{-0.25}$.

2.3.2.2 Mass loss prescription Based on the MHD mass loss profile, we express the mass loss term in the continuity equation as

$$\dot{\Sigma}_{\rm wind} = \bar{b}\frac{\Omega_{\rm p}}{2\pi}\Sigma, \tag{18}$$

where $\bar{b}$ is the mass loss rate. The mass loss rate is equivalent to the torque coefficient b away from the planet, but reduced to zero near the planet according to

$$\bar{b} = \begin{cases} b & \text{if } |r - r_{\rm p}| > 1.0\ r_{\rm H} \\ 0 & \text{otherwise} \end{cases} \tag{19}$$

where $r_{\rm H}$ is planet's Hill radius. The mass loss is reduced to zero in the planet gap to reflect that there is no mass loss in that region. The surface density dependence is intended to capture the mass loss rate peaking near the location with the highest density at each gap edge, and also helps smooth the discontinuity between the two regions. We neglect the small mass inflow in the gap because we find that the gap already depletes too slowly compared to the MHD simulations. We also neglect that the mass loss rate outside of the gap is non-uniform and not exactly proportional to the surface density because our main focus to approximate the profile the best near the outer gap edge.

2.3.2.3 Viscosity prescription Besides including the two main effects of the wind, we also account for turbulence in the disc. Even though the level of turbulence should not be too important for accretion relative to the wind, we anticipate it may have a stronger effect on the gap profile.

We presume that the Maxwell stress $\mathcal{T}_{{\rm r}\phi}^{\rm Max}$ has two components, a primary component that induces laminar accretion and a secondary component that induces a low amount of turbulence. To keep the turbulent component of the overall accretion small, we prescribe a small constant $\nu = 10^{-5}\ r_{\rm p}^2 \Omega_{\rm p}$. For simplicity, we drop the units of ν hereafter. The viscosity is kept constant to keep the model simple and to make it easier to compare to viscous studies in which it is use a constant viscosity. We note that although $\mathcal{T}_{{\rm z}\phi}$ drives more accretion than an $\mathcal{T}_{{\rm r}\phi}$ of equal magnitude, that extra factor has already been absorbed into b. In our model, the wind-driven and viscous accretion rates relate through the ratio $\dot{M}_{\rm b}/\dot{M}_\nu = (b/\nu)/\pi$.

2.3.3 Reference prescribed model

To understand if our model and its components have any effect on the gap profiles, we compare our model to the one developed by K20, which contains two components: a torque prescription and a mass loss prescription.

The torque term in the K20 model is given as

$$\Gamma = \dot{\Sigma}_{\rm wind}\Omega_{\rm K} r^2 (\lambda - 1), \tag{20}$$

taken from their Equation 5. The lever arm λ is set to their fiducial value of $\lambda = 2.25$. There are two key differences. The main one is the resulting power law in the radial direction of the torque. Their torque follows a $\Gamma \propto r^{-2.25}$ profile, whereas the torque in our model follows a flatter $\Gamma \propto r^{-1.5}$ profile. A more minor difference is that we do not include the lever arm.

The mass loss term in the K20 model is

$$\dot{\Sigma}_{\rm wind} = b\frac{\Omega_{\rm K}}{2\pi}\Sigma, \tag{21}$$

taken from their Equation 3, where b serves the same purpose and is the basis for our definition of b. There are two slight differences. First, they apply the mass loss everywhere, whereas we only apply it outside the gap. Second, their mass loss rate depends on the local orbital period, which we neglect in order to boost the mass loss rate at the pressure bump.

The orbital dependence in the mass loss term does not make a significant difference in short-term simulations around several hundred orbits or less, but it does in long-term simulations around 1000 orbits or more. In particular, the outer disc depletes much more slowly away from the gap with the K20 prescription. Since their prescription is better physically-motivated in the longterm, we do include the orbital dependence in our long-term simulations, as we discuss in Section 4.3.

Lastly, in some cases, we also add in the viscosity and extra gap torque components from our model for comparison purposes.

2.4 Simulations

All of our simulations are run with the FARGO3D hydrodynamic code (Benítez-Llambay & Masset 2016; Benítez-Llambay et al.

2019). In our fiducial runs, we carry out 2D simulations generally following the setup choices from A&B 2023. For that reason, the gas surface density distribution follows a power law of $\Sigma_0(r) = \Sigma_p(r/r_{\rm p})^{-p}$, the initial surface density at the location of the planet is $\Sigma_{\rm p} = 2.315 \times 10^{-4}\ M_\star r_{\rm p}^{-2}$, the surface density power law is $p = 1.25$, and the disc has a flat aspect ratio of $h = 0.1$. The initial dust profile matches the gas power law, except with a 1-to-100 dust-to-gas ratio. Nevertheless, as we neglect self-gravity, our fiducial simulations are scale-free with respect to the density for both the gas and dust. The only set of cases in which the density level can affect the results is with a migrating planet. The dust Stokes number is set to ${\rm St} = 0.023$, which is chosen as an intermediate grain size to monitor the appearance of the dust in vortices. For our main purpose of studying the gap profiles, the dust is not used.

Our fiducial simulations have an arithmetic grid spanning from $r \in [0.3, 4.0] r_{\rm p}$ = $[r_{\rm in}, r_{\rm out}]$ in radius and full-circle in azimuth ϕ. The domain has 768 grid cells in both directions. With this radial resolution, the scale height of $H = 0.1\ r_{\rm p}$ at the location of the planet is resolved by 21 grid cells, about the same as the 20-grid-cell maximum resolution used by A&B 2023. Such a resolution should be sufficient for studying the gap profiles. However, a more in-depth study focusing on the vortices (and the dust in particular) may require a higher resolution. We chose a relatively low resolution both to match the MHD study and to test the efficacy of our model with an efficient setup that does not require extensive computational time.

At the boundary, we have wave-killing zones, known in FARGO3D as Stockholm boundary conditions (e.g. de Val-Borro et al. 2006). The inner boundary zone exists from $0.3\ r_{\rm p} < r < 0.375\ r_{\rm p}$, with the end at $1.25\ r_{\rm in}$. The outer boundary zone exists from $3.36\ r_{\rm p} < r < 4.0\ r_{\rm p}$, with the start at $0.84\ r_{\rm out}$. The damping timescales in both regions are $\tau = 0.3\ \Omega^{-1}$. We found that our fiducial results with the prescribed wind are not heavily dependent on the boundary conditions. On the other hand, the gap profiles can change by a significant amount without wave-killing zones if there is also no prescribed wind.

3 MATCHING MHD GAP PROFILES

With a four-component prescribed disc wind model, we can reasonably match the 3D MHD gap profiles using a 2D hydrodynamic model for cases with a high-mass planet above the thermal mass and the fiducial high aspect ratio of $h = 0.1$. Our prescribed model consists of

(i) a background torque power-law profile,
(ii) a mass loss profile,
(iii) viscosity, and
(iv) enhanced torque in the planet gap.

As expected, the extra torque in the gap is the key component to deepen the gap enough to match the high gap depths from the MHD simulations. Meanwhile, the viscosity is the key component to match the gap profile at and around the outer gap edge. In general, the gap-opening process with 2D hydrodynamics is much slower than in 3D MHD. Consequently, we find a better match between the final MHD gap profile from A&B 2023 at 140 orbits with our 2D hydrodynamic gap at about 210 orbits.

Our best fit for the gap profiles uses the level of background torque taken from the MHD simulations. On the other hand, the level of viscosity is about one-sixth the level of stress from the MHD simulations, suggesting the Maxwell component that dominates the stress is largely laminar (i.e. five-sixths not turbulent).

There are only a narrow range of values for the viscosity that could be viable. If the viscosity is too high, it would become the main driver of accretion in the disc. It could also prevent the formation of vortices at the outer gap edge, which do appear in the MHD simulations and fundamentally alter the gap profile. If it is too low, it would let the planet push too much material away from the outer gap edge and prevent the pressure bump from becoming as strong as the ones in MHD.

We were not able to develop as adequate of a fit for the gap profiles induced by lower-mass planets. With lower-mass planets, the pressure bump at the outer gap edge already has too high of a density even with no viscosity. Adding in viscosity only worsens this problem. As such, no amount of constant viscosity results in a good fit.

3.1 Context

We chose the intermediate-mass case from A&B 2023 with a 3 Jupiter-mass (3 thermal-mass) planet as our fiducial case. We aim to fit the gap itself and the general outer gap edge profile, focusing on three main quantities: the gap depth, the outer gap edge location (i.e. the gap width or half-width), and the surface density at the outer gap edge. The last two quantities are measured at the peak in the pressure bump.

We do not focus on any quantities related to the inner gap edge because A&B 2023 found a purely MHD-driven gap near there, located at about $r = 0.5\ r_{\rm p}$ (as shown in their Figure 3, and re-plotted in many of the figures in this work). This additional gap affected the planet's gap structure towards its inner gap edge. Since this feature is not related to the planet and could appear in a different location or not at all in a real disc, we do not attempt to reproduce the inner gap edge and only focus on the gap itself and the outer gap edge.

We expect that if we could match all three quantities, the rest of the profile would also match (aside from the inner gap edge). We chose the location of the pressure bump as the best way to measure the gap width because it can be inferred directly from dust observations. The importance of the gap edge density is that it has some correlation with whether vortices could form through the Rossby Wave instability (e.g. Lovelace et al. 1999; Ono et al. 2016). We consider the gap depth important because many studies of gap profiles in viscous wind-less discs have focused on developing analytical scaling relations for the gap depth (Fung et al. 2014; Duffell 2015; Kanagawa et al. 2015).

A&B 2023 already attempted to fit their MHD gap profiles with 2D hydrodynamic simulations, but without any prescribed disc wind model. For each of their main three cases (1, 3, & 5 Jupiter-mass), they ran two comparison cases: one inviscid and one viscous with $\alpha = 6 \times 10^{-3}$, the measured background value in their simulations, which is largely determined by the Maxwell stress. Of the two, they advocate for the inviscid case as the better simple fit, citing its deeper gap and its matching gap width near half-max on the exterior side of the gap.

Despite those successful parts, neither of the simple fits appeared adequate. Even though the inviscid gap was deeper, both gaps were noticeably too shallow. Additionally, the gap width in the inviscid case only matched the MHD case along the "shoulder" of the outer gap edge. However, if one matches the gap width based on the location of the peak in the pressure bump instead — since this sets the gap width in mm dust observations — then their viscous case actually performs better than the inviscid case, owing to

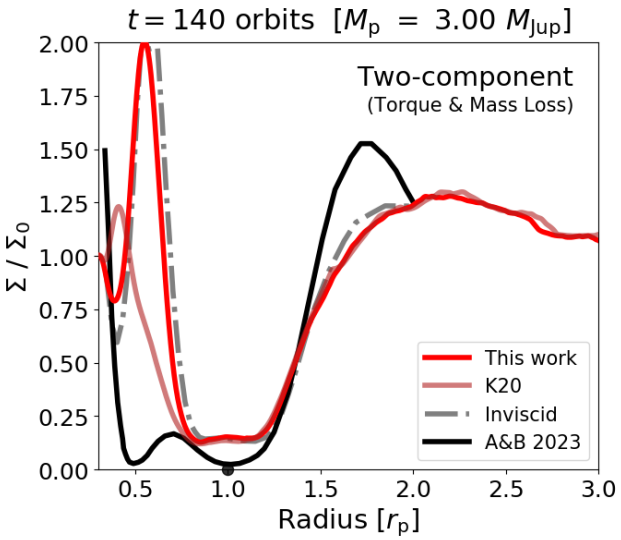

Figure 2. Comparison of the two-component prescribed disc wind models from this work (*red*) and by K20 (*light red*) to the MHD simulation (*black*) by A&B 2023 and their inviscid comparison run (*grey dashed line*), all at $t = 140$. The two-component models are nearly identical to the inviscid comparison run, and neither does a particularly good job at matching the real MHD gap profile at the trough of the gap or the outer gap edge. The two models themselves are even more identical to each other at $r > 0.8\,r_p$.

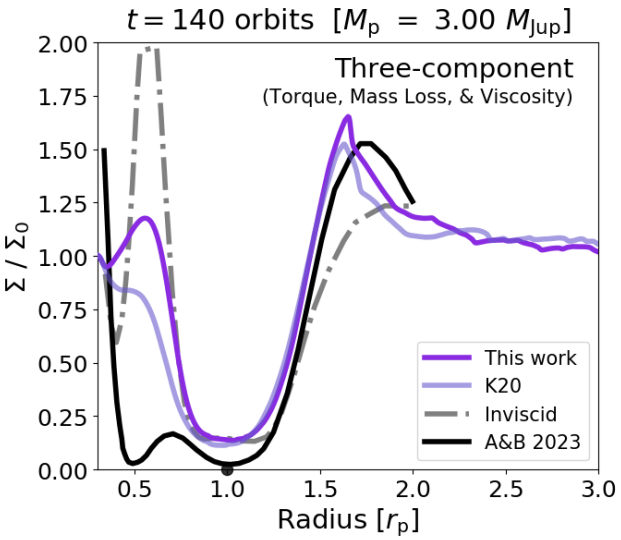

Figure 3. Comparison of three-component prescribed disc wind models from this work (*purple*) and by K20 (*light purple*) to the MHD simulation (*black*) by A&B 2023 and their inviscid comparison run (*grey dashed line*), all at $t = 140$. The three-component models are much closer to matching the real MHD gap profile than the two-component models, particularly at the outer gap edge.

the inviscid pressure bump spreading out way too far away from the planet.

3.2 Building up the best-fit model

In this section, we build up our best-fit model starting out from the two-component prescription with torque and mass loss and then showing how the gap profiles change when adding in viscosity as a third component and extra gap torque as a fourth. At each level of complexity, we compare the gap profiles for both our model and the K20 model to the MHD gap profiles at $t = 140$, the end time of the simulations by A&B 2023. Afterwards, we extend the comparisons of the gap profile to the full evolution over time. We then discuss the roles of the vortices and the inner MHD gap. At the end, we show how varying any of the parameters only worsens the quality of the fit.

We begin with the two-component models that consist of a prescribed torque and mass loss. Figure 2 compares the gap profiles from the two prescribed models to the MHD gap profile. With just the torque as the main component, the prescribed wind has little effect on the gap profile. The resulting profiles largely match the inviscid comparison run by A&B 2023, which is not entirely surprising since neither simulation has viscosity. The mass loss component also has little effect on the gap profile exterior to the planet because of the slow dependence on the orbital timescale. As with the inviscid run, the primary outcomes of the two-component model that could be improved are that the amplitude of the pressure bump and the depth of the gap should be increased.

To make the peak of the pressure bump higher, we added viscosity as a third component. As Figure 3 shows, incorporating viscosity significantly elevates the pressure bump. With a value of $\nu = 10^{-5}$ (equivalent to $\alpha = 10^{-3}$ at $r = r_p$), not only is the peak of the gap edge much closer to the target location and density from the MHD run, the slope of the inner shoulder of the outer gap edge matches almost perfectly across the entire shoulder.

The amount of viscosity we use helps match the MHD gap profile in two different ways. First, without any viscosity, there was nothing to oppose the planet driving material away from it. Having viscosity, however, stops that material from spreading out too far from the planet, keeping the pressure bump as strong as it is in the MHD run. Second, our viscous model also works better than the comparison run by A&B 2023 because we use a lower level of viscosity. That lower amount allows vortices to develop at the gap edge through the Rossby wave instability (RWI: Lovelace et al. 1999; Li et al. 2000, 2001), which also occurs in the MHD run. The viscous comparison run they did was less effective because it used too high of a viscosity, which suppressed the RWI and prevented vortices from ever forming. With the three-component model, the main issue remaining at the outer gap edge is that it is slightly too close to the planet.

To make the trough of the gap deeper, we added in extra torque in the gap as a fourth component. As Figure 4 shows, the extra torque does indeed make the gap deeper with our model, although still not as deep as the MHD run. Unlike with our model, the extra torque does not actually make gap deeper with the K20 model, as highlighted in Figure 5. Another minor improvement is that the location of the pressure bump and general shape of the gap profile there are slightly better with our model than the K20 model.

Even though our four-component model already does well to match the MHD gap profile, we can get even better matches if we continue the simulation. As shown in Figure 6, the gap profile at the outer edge at $t = 163$ orbits just about perfectly matches the MHD simulation at $t = 140$ orbits, including the entire inner shoulder up to and past the peak of the pressure bump. The only part left to match is the trough. Once the gap reaches $t = 214$ orbits, the trough of the gap also just about matches the gap depth reached at the end of the MHD simulation. Meanwhile, the profile at the outer gap edge still aligns, creating a near-perfect match in the entire re-

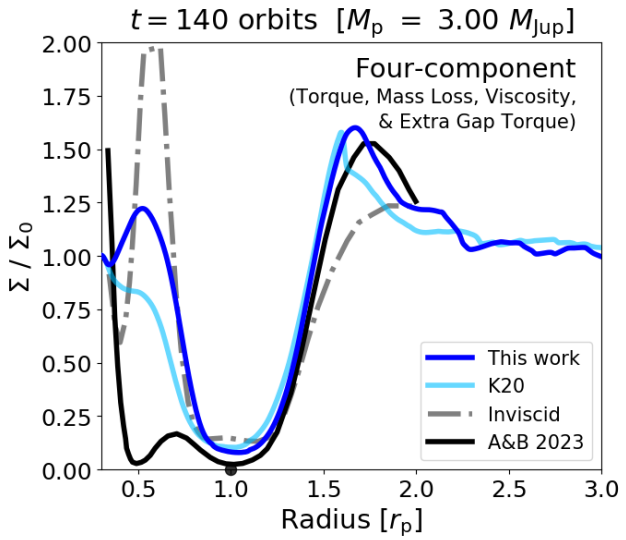

Figure 4. Comparison of the four-component prescribed disc wind models from this work (*blue*) and by K20 (*light blue*) to the MHD simulation (*black*) by A&B 2023, and their inviscid comparison run (*grey dashed line*), all at $t = 140$. The modified four-component model is closer than the original to the MHD, both in having a deeper gap and also in having its pressure bump slightly weaker and further out.

gion exterior to the planet. This "delay" of about 70 orbits to almost perfectly match the gap profile is consistent with the gap itself opening much slower, as we discuss in the next section. Overall, we conclude our four-component model can achieve a near-perfect match to the MHD gap profile, albeit at a noticeable delay.

3.3 Gap profile evolution over time

Although we find a reasonably good fit to MHD gap profile near the end of the MHD simulations, the fits earlier on the simulation were not as good. At the very beginning, the differences between our best-fit prescribed model and the MHD gap profiles are the largest. These differences lessen over time, as illustrated in Figure 8. In particular, there are three main differences that the prescribed models do little to help address.

First, the gap deepens much more quickly with MHD than with the prescribed models. Second, the MHD gap profiles are much more symmetric than the ones with the prescribed models. Third, the gap profiles with the prescribed models much more clearly open double gaps with both troughs located away from the planet. In contrast, the MHD gap profiles have a trough at the location of the planet from the onset or close. Each of these discrepancies dwindle over time as the gap gets deeper, but are still at least somewhat noticeable by the comparison point at the end of the MHD simulations.

The double gap, as well as the speed at which the gap deepens, both relate to how the gap depletes. In our simulations, some of the gas remains trapped at the L5 Lagrange point 60° co-orbital behind the planet. Gas collects here because a vortex-like structure develops at the L5 point, a well-known phenomenon in hydrodynamic simulations with a planet (e.g. Montesinos et al. 2020). This gas at L5 both creates the double gap and slows the depletion of the gap. In contrast, the extra torque caused by the wind in the MHD simulation helps clear out all of the material in the gap, even at the L5 point. Even with the extra torque in our prescribed model, we do not see that happen in our simulations. As a result, the MHD gap profiles deepen much quicker than ours, especially at the onset.

That quickness is somewhat surprising given that the density in the gap isn't that much lower at the onset. We had expected that the gap would not deplete faster until much later because the extra torque in the gap is expected to arise from the gap's much lower density. This early discrepancy is why we such high $K_{\rm gap} = 5$ level of extra torque in the gap and do not use any tapering or density dependence near the beginning. The level recommended by A&B 2023 was $K_{\rm gap} = 3$ to 5, but even with the high level we use, our gaps still lag behind, most noticeably in the gap depth. That lagging may suggest the deeper gaps are not just due to the extra torque in the gap because it shouldn't arise so early on.

3.4 Different planet masses

Like our fiducial test case, we can reproduce the gap profiles for the 5 Jupiter-mass (5 thermal-mass) planet case, the highest-mass planet simulated by A&B 2023 reasonably well with the same model parameter values. Figure 9 shows how the gap profiles match up. Without any prescribed wind or viscosity, the gap edge shoulder already follows the MHD reasonably well, but the biggest difference is the gap itself is way too shallow. Like with a 3 Jupiter-mass planet, the viscosity similarly helps strengthen the pressure bump at outer gap edge, while the extra gap torque helps deepen the gap. One small difference is that that the outer gap edge has the correct amplitude without mass loss. Adding in mass loss drops the amplitude a bit so that the full model better aligns with the inviscid case near the gap edge than the MHD. The main strengths are that the shoulder and gap edge location align with the MHD gap profile almost perfectly, just like in the fiducial case.

On the other hand, the gap profiles for the lowest-mass case with a 1 Jupiter-mass (1 thermal-mass) planet are much more difficult to reproduce. Figure 10 compares the gap profile for this case to the corresponding viscous and inviscid comparison runs by A&B 2023. Unlike in the higher-mass planet cases, the inviscid pressure bump at the outer gap edge is actually higher amplitude than the MHD, not lower. The pressure bump does not end up as weak because the planet is too low-mass to push the pressure bump away from it. With the pressure bump already too strong, adding in viscosity does not help the way it does in the higher-mass planet cases. It does weaken the pressure bump like the MHD; however, the profiles still generally do not come close to matching, mainly because of the trough. The gap depth is underestimated by such a large amount that it does not matter if the viscosity helps improve profile at the outer gap edge. With the structure in the gap itself being so different, the gap profile as a whole ends up with a fundamentally different structure.

We see that issue of an underestimated gap depth messing up the entire gap profile in the higher-mass planet cases as well, but only at earlier times. In those cases, however, the planet is massive enough that the gap eventually becomes much deeper later on. As a result, the gap depth in our simulations and the MHD simulations eventually converge to about the same level, even if the percentage difference between the two is still large. With a lower-mass planet, the gap is much shallower and thus, the large percentage difference between the two still has a significant effect on the rest of the gap profile.

Overall, we can reproduce the high-mass planet gap profiles reasonably well, but cannot match the lower-mass case. We find it promising that we can reproduce the gap profiles with the same model parameters for both the 3 $M_{\rm Jup}$ and 5 $M_{\rm Jup}$ cases even

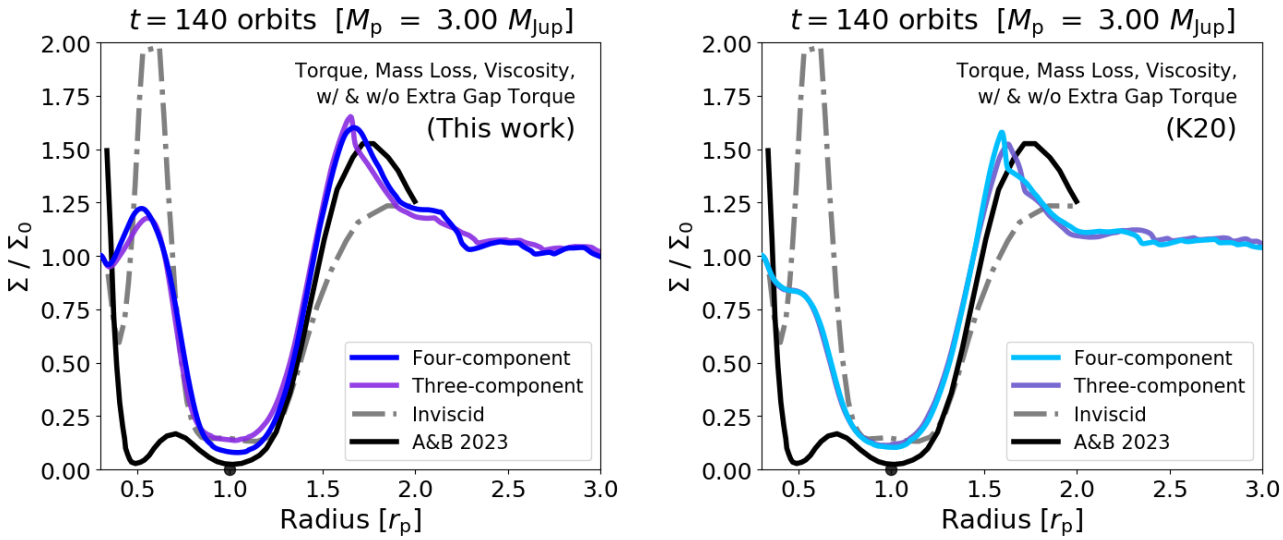

Figure 5. Comparison of the three-component and four-component prescribed disc wind models from this work (*left: blue and purple*) and by K20 (*right: light blue and light purple*), the MHD simulation (*black*) by A&B 2023, and their inviscid comparison run (*grey dashed line*), all at $t = 140$. There is a noticeable difference in the gap depth with the model from this work, but no noticeable difference with the K20 model.

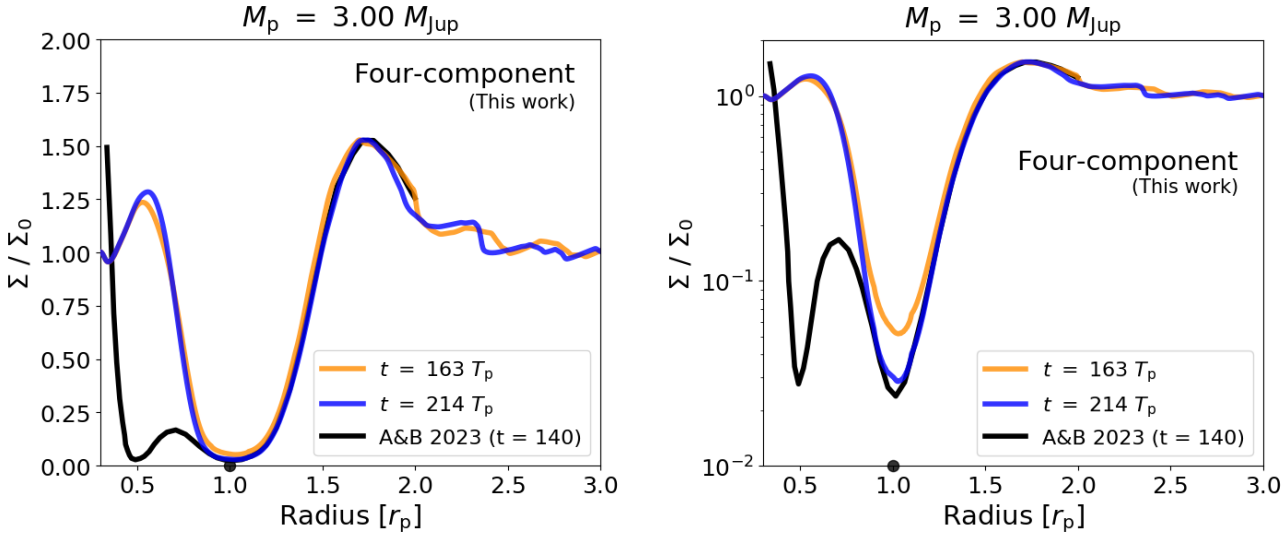

Figure 6. Comparison of the four-component prescribed disc wind model from this work at $t = 163$ (*orange*) and $t = 214\ T_p$ (*blue*) to the MHD simulation (*black*) by A&B 2023 at $t = 140\ T_p$. At $t = 163$, the outer gap edge matches perfectly. At $t = 214$, the entire outer region – both the trough and the the outer gap edge – matches perfectly.

though there are moderate differences in the MHD runs between their measured profiles for α, torque, and mass loss.

We do not think it is surprising that the low-mass case is more difficult to match because the planet is only at the thermal mass. We interpret the feasibility of which gap profiles we can match as evidence that the more massive planets play a more dominant role in shaping the gap structure. When the planet is lower mass and barely able to open a gap, the wind plays a more integral role in shaping the gap structure, making it more difficult to capture the MHD effects associated with the wind with just a prescription.

3.5 Role of vortices

Our main interest in prescribed disc winds was to see if they can match the 1D MHD planetary gap profiles, but the gap profiles themselves are not truly 1D due to vortex formation at the gap edge.

In general, vortices can arise at planetary gap edges (Li et al. 2005; Hammer et al. 2017, 2021; Hammer & Lin 2023) through the Rossby Wave instability if the disc has sufficiently low viscosity (de Val-Borro et al. 2007). The specific criteria that makes the disc unstable to the RWI is an inverse vortensity maximum becoming too sharp (Lin 2012; Ono et al. 2016), where the inverse vortensity is surface density Σ divided by vorticity $\omega = (\vec{\nabla} \times \vec{v})_z$. That criteria may be satisfied at the maximum located nearly coincident with the pressure bump at a gap edge. However, higher vis-

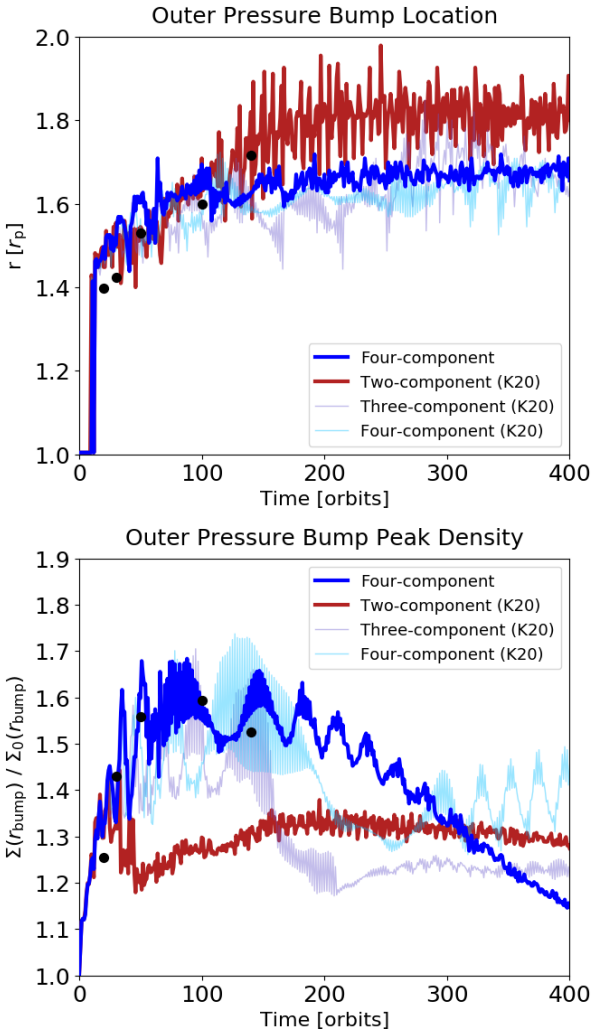

Figure 7. Gap edge location (*top*) and gap edge density (*bottom*) over time with different numbers of components to the prescribed wind. The values from A&B 2023 (*black dots*) at five different times are shown for comparison. All of the models except the basic two-component model with no viscosity match the gap edge density and position reasonably well, indicating viscosity is the key component to match these features.

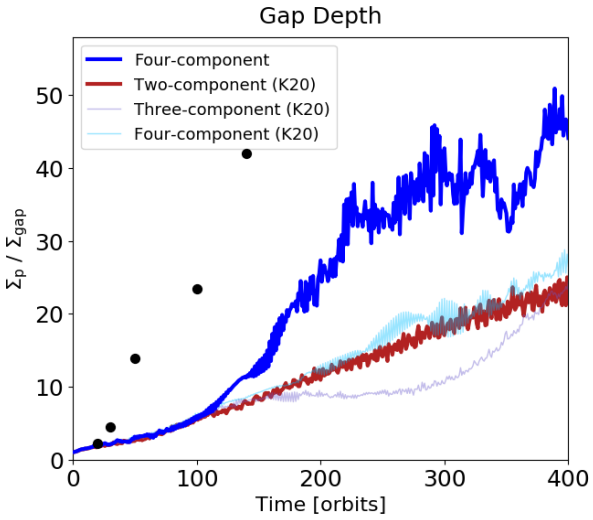

Figure 8. Gap depth over time with different numbers of components to the prescribed wind. The values from A&B 2023 (*black dots*) at five different times are shown for comparison. The full four-component model with the new torque profile is the only fit that approaches the depth reached with MHD, albeit with a time delay.

cosities can smooth out the gap edge enough to prevent the RWI from occurring. The resulting vortices can be compact or elongated, which largely depends on whether the local Rossby number $\mathrm{Ro} = (\vec{\nabla} \times (\vec{v} - \vec{v}_\mathrm{K}))_z / 2\Omega$ is above or below the critical value of -0.15 respectively (Surville & Barge 2015; Hammer et al. 2021).

Like in the MHD simulations by A&B 2023, all of the planets in our fiducial simulations trigger vortices. Also like their work, the two higher-mass planets trigger stronger vortices, as depicted in Figure 11, while the lowest-mass planet triggers a noticeably weaker vortex, as depicted in Figure 12. The stronger vortices are compact with $\mathrm{Ro} < -0.15$, while the weaker vortex is elongated. The stronger vortices last about 400 to 500 orbits in both the gas and dust, while the weaker vortex lasts about half as long at around 200 orbits. All of the vortex lifetimes are relatively short because of the relatively high viscosity.

As the MHD simulations have vortices, it would be ideal if our simulations had vortices with similar morphologies in order to match the gap profiles. Vortices can affect the gap profiles in a few ways. They can transport material outwards from along the outer gap edge shoulder into the vortex itself when the instability is triggered. If they are compact, they can also drive accretion as their spiral waves transport angular momentum.

Allowing vortices to occur by not having too high of a viscosity indeed helps us match the profiles for the highest-mass planets, but not the lower-mass one. We believe the lower-mass one still does not match for two main reasons. First, the trough of the gap is way too shallow compared to the MHD and that has little to do with the vortex. Second, the vortex itself is elongated and with this weaker structure, it does not have as much effect on the gap profile.

3.6 Role of inner MHD gap

One of the main differences between our prescribed disc wind model and the disc wind simulations by A&B 2023 is the secondary MHD-driven gap located interior to the planet. We ignored this feature entirely in our fiducial simulations and were still able to reproduce the rest of the gap structure away from this feature, albeit at a time delay, particularly for the depth of the gap. As such, we were interested in investigating whether the MHD gap could be partially responsible for the time delay in the opening of the gap.

As we were unable to prescribe an inner MHD gap, we instead tested what would happen if we expanded the planetary gap region to include more of the interior region of the disc. Specifically, rather than apply the extra gap torque at a level $K_\mathrm{gap} = 5$ in just the usual region, we also applied it in the inner part of the disc over a range $r_\mathrm{gap,in} \leqslant r \leqslant r_\mathrm{p}$, leaving out smoothing at the inner edge. We tested three values of $r_\mathrm{gap,in} = 0.45$, 0.65, and 0.85 r_p. This setup mimics the later stages of the MHD simulations where the planetary gap and inner MHD gap have some overlap. It may not capture what happens in the early stages of the MHD simulations before there is any overlap. As Figure 13 shows, the planetary gap does indeed open up much faster when it encompasses more of the inner disc, supporting the notion that the MHD gap contributes to the gap deepening at a faster rate.

We note that although the inner MHD gap appears to help

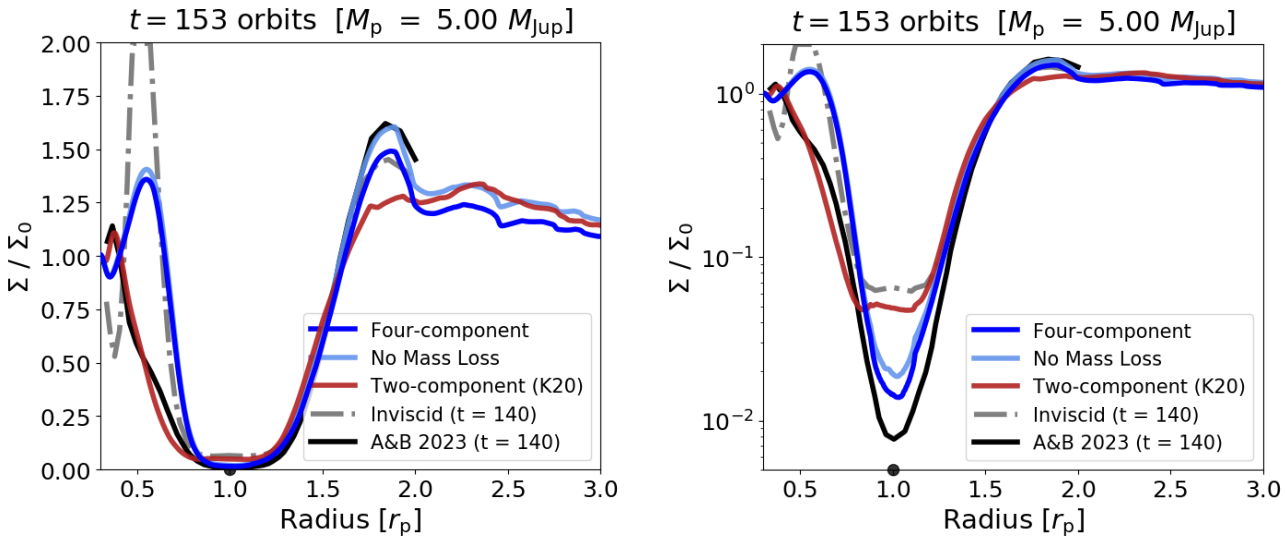

Figure 9. High-planet-mass comparison of the modified four-component (MHD-based torque, MHD-based mass loss, viscosity & extra gap torque) prescribed disc wind model (*blue*) to the same model except without mass (*cornflower blue*), and the K20 model (*red*) all at $t = 153$, as well as the MHD simulation (*black*) by A&B 2023 and their inviscid comparison run (*grey dashed line*) at $t = 140$. The planet mass is 5 $M_{\rm Jup}$. Like at intermediate planet mass, the viscosity elevates the pressure bump at the outer gap edge. Unlike at intermediate planet mass, the case without mass loss gives a better fit while the case with mass loss better resembles the inviscid run.

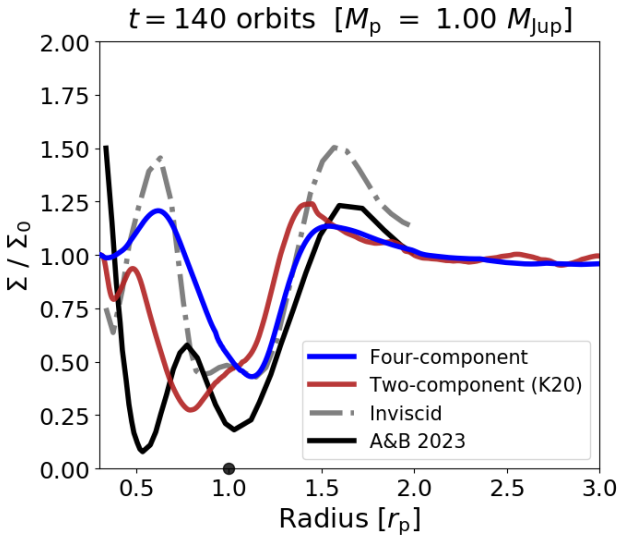

Figure 10. Low-planet-mass comparison of the modified four-component (MHD-based torque, MHD-based mass loss, viscosity & extra gap torque) prescribed disc wind model (*blue*) to the K20 model (*red*), as well as the MHD simulation (*black*) by A&B 2023 and their inviscid comparison run (*grey dashed line*) at $t = 140$. The planet mass is 1 $M_{\rm Jup}$. Unlike at intermediate planet mass, viscosity does not elevate the pressure bump at the outer gap edge and as a result does not help produce a better fit.

deepen the gap, it is not the sole reason for the gap opening more slowly. As we had already pointed out, the lack of depletion of the gas at the Lagrange point also contributes to the slower gap-opening process, particularly at earlier times before it depletes.

3.7 Alterations to best-fit model

Our best-fit model uses the wind strength $b = 5 \times 10^{-4}$ taken from the simulations by A&B 2023 and a viscosity $\nu = 10^{-5}$ approximately one-sixth the level from their work. To show these values produce the best fit, we also tested other higher and lower values for both parameters.

With different viscosities, we observe three expected regimes, as shown in Figure 14. At high levels, the viscosity dominates over the wind and is the main factor determining the shape of the gap profile aside from the mass loss. The high viscosity also suppresses vortices, resulting in a fundamentally different gap structure where the gap is more much shallow and the outer gap edge has a different shape. At low viscosity, the wind dominates over the viscosity, leaving the gap profile mainly determined by the wind and the vortices that exist. The gap is deeper and the outer pressure bump is further from the planet. Our fiducial model lies in-between at intermediate viscosity, where the wind-driven accretion rate is higher than the viscosity-driven accretion rate (see Section 2.3.2.3), but the viscosity is still strong enough to matter. The gap depth reaches an intermediate value, while the amplitude of the outer gap edge is actually stronger than with higher or lower viscosity.

With different wind strengths, we see a smoother transition in the gap profiles from higher to lower values, as shown in Figure 15. Stronger winds create a much weaker pressure bump and a much deeper gap. At $t = 163$, the stronger wind already has the correct gap depth, in contrast to our fiducial model. We still prefer our fiducial model, however, because we believe the L5 gas and the lack of an inner MHD gap are the reasons the gap depth is underestimated.

4 EXTENSIONS

Now that we have tested our prescribed disc model against the MHD simulations on which it is based, we apply it to a wider parameter space and longer simulations. We test the model's applicability while also exploring the potential effects of having a disc

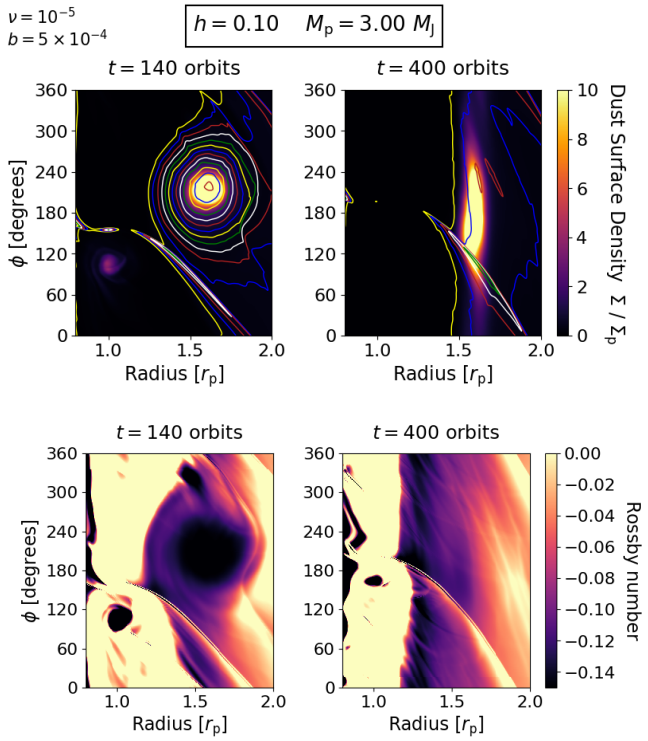

Figure 11. Snapshots showing the evolution of the the dust density (*top panels*) and Rossby number (*bottom panels*) in the presence of a super-thermal mass planet ($M_p = 3.0\ M_{Jup}$) in a disc with our fiducial full wind model ($b = 5 \times 10^{-4}$ and $\nu = 10^{-5}$). Gas density contours (at $\Sigma/\Sigma_p = 0.4, 0.5, 0.6$, etc.) are overlaid. The vortex is compact but quickly fades before 500 orbits due to the high viscosity.

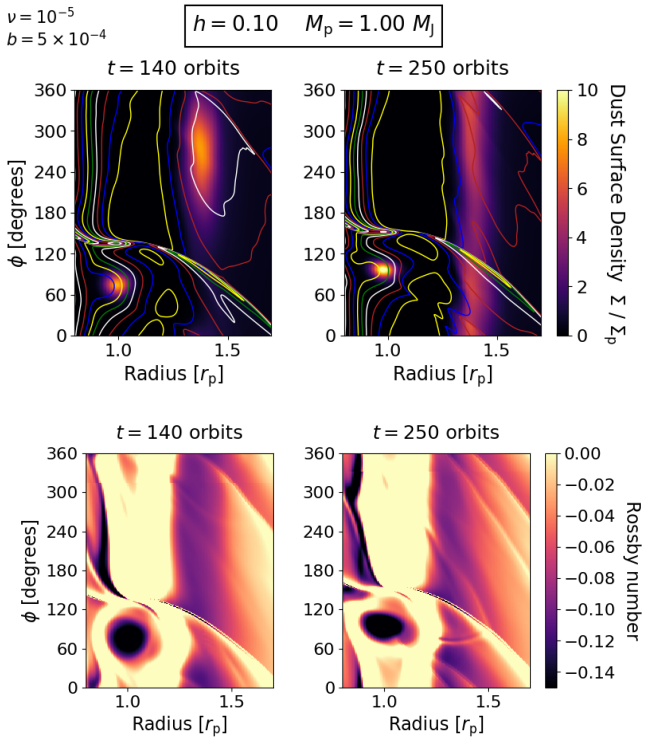

Figure 12. Snapshots showing the evolution of the the dust density (*top panels*) and Rossby number (*bottom panels*) in the presence of a thermal mass planet ($M_p = 1.0\ M_{Jup}$) in a disc with our fiducial full wind model ($b = 5 \times 10^{-4}$ and $\nu = 10^{-5}$). Gas density contours (at $\Sigma/\Sigma_p = 0.4, 0.5, 0.6$, etc.) are overlaid. The vortex is elongated and spreads into a ring by around 250 orbits in both the gas and dust.

wind in regimes beyond what the MHD simulations have explored so far. These tests require minor modifications to the setup that are described directly in the relevant subsection.

4.1 Varying disc parameters

With the new prescribed model capable of reproducing gap profiles for high-mass planets and a relatively thick disc aspect ratio of $h = 0.1$, we now test whether it can do the same at thinner aspect ratios of $h = 0.05$ and 0.08. For each of these two aspect ratios, we test four cases:

(i) our full prescribed model,
(ii) a control case with just our fiducial viscosity,
(iii) a control case with just the wind and no viscosity, and
(iv) a control case with neither the wind or viscosity.

Although we do not have MHD simulations to compare to for these thinner discs, we can still compare the prescribed wind model to wind-less viscous and inviscid counterparts to see if the same trends occur.

For the thinnest disc at $h = 0.05$, we find that the trend between the different models better resembles the low-mass 1 M_{Jup} case that we could not reproduce. In particular, the inviscid simulation produces the strongest pressure bump, stronger than either the viscous case or the prescribed model, as illustrated in the top panel of Figure 16. As such, adding viscosity to the prescribed model no longer helps strengthen the inviscid pressure bump because it is already too strong.

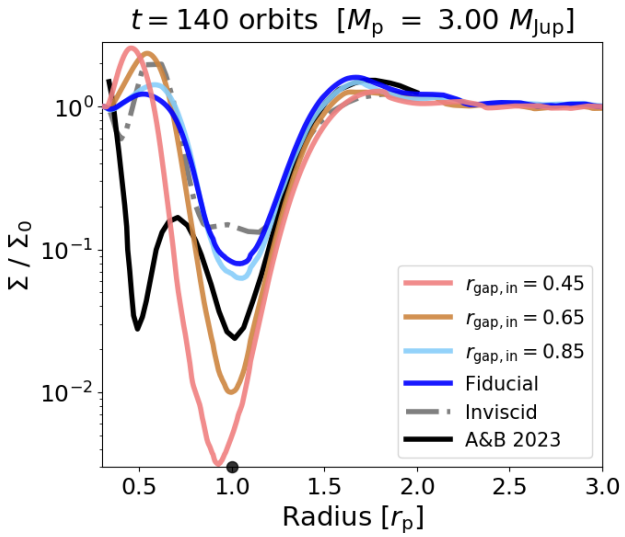

Figure 13. Gap depth comparison with different-sized "gaps" for where the extra gap torque is applied. The outer edge of the gap is normal, while the inner edge is moved inwards to $r_{gap,in}$ as a crude way to resemble the MHD gap from A&B 2023. With more gas cleared out interior to the planet, the entire planetary gap becomes much deeper. As such, the lack of an MHD gap in our fiducial case may explain part of why the gap is shallower.

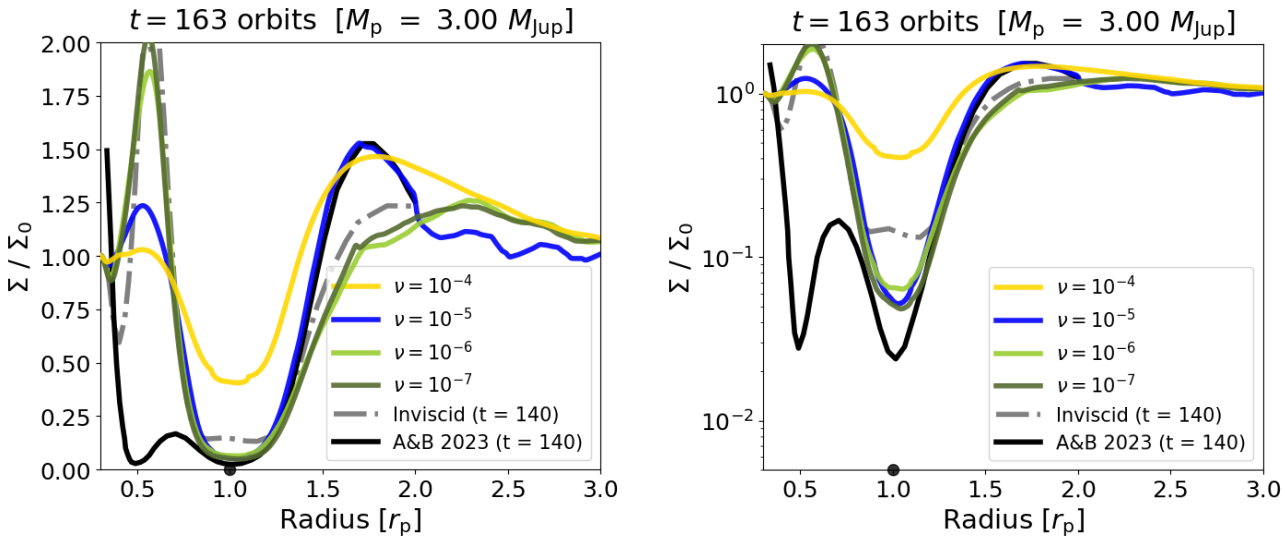

Figure 14. Comparison of the modified four-component (MHD-based torque, MHD-based mass loss, viscosity & extra gap torque) prescribed disc wind model (*blue*) to the same model with different viscosities all at $t = 163$, as well as the MHD simulation (*black*) by A&B 2023 and their inviscid comparison run (*grey dashed line*) at $t = 140$. With higher viscosity, the amplitude of the pressure bump increases while the amplitude of the gap depth decreases (although the latter effect is not as strong until later times).

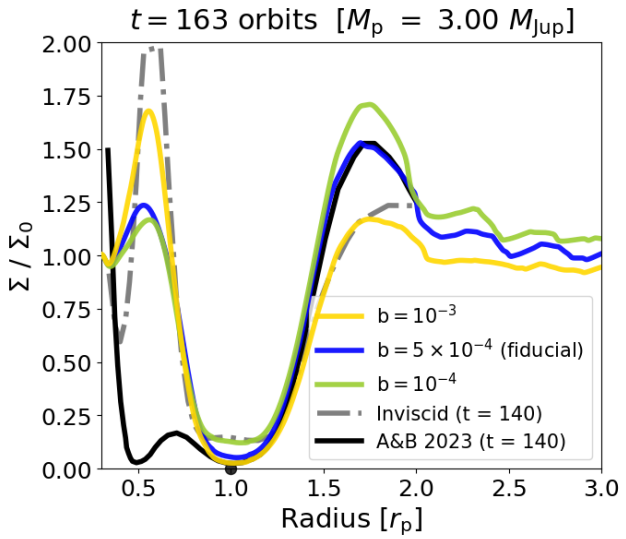

Figure 15. Comparison of the modified four-component (MHD-based torque, MHD-based mass loss, viscosity & extra gap torque) prescribed disc wind model (*blue*) to the same model with different wind strengths all at $t = 163$, as well as the MHD simulation (*black*) by A&B 2023 and their inviscid comparison run (*grey dashed line*) at $t = 140$. With stronger winds, the amplitude of the pressure bump drops and the amplitude of the gap depth increases.

We believe our prescribed model fares slightly better with the intermediate aspect ratio of $h = 0.08$. Although the viscosity still does not help elevate the pressure bump, at the very least the pressure bump does not drop either. Instead, the pressure bump location and amplitude are about the same with our full model as in the inviscid control case with no wind, which is illustrated in the bottom panel of Figure 16. The gap edge shoulder is one part that is different, owing to the gap being deeper in the case with our full model. Overall, the trends for this set of cases is a bit different from the $1\ M_{Jup}$ case, although it still does not follow the trend from the 3 or $5\ M_{Jup}$ cases that we could reproduce.

Since we could not reproduce the $1\ M_{Jup}$ case and the only cases we could reproduce are the ones where the viscosity elevates the outer gap edge pressure bump, we are less optimistic about the ability of our model to reproduce gap profiles at lower aspect ratios. It may still be possible for our model to work, though, since we believe the trough not being deep enough is one of the key reasons we cannot reproduce the $1\ M_{Jup}$ gap profile. As such, for our model to have success at lower aspect ratios, we think that success would be more likely with more massive planets that open gaps deep enough for the trough discrepancy not to matter.

4.2 Vortex trigger criteria

For planets to trigger vortices at their gap edges when they open up gaps, the disc must have a sufficiently low viscosity. It has been suggested that magnetic disc winds can help alleviate this restriction and allow stronger vortices to form at higher viscosities than usual (Wu et al. 2023). As that was done with a variant of the K20 model first introduced by Elbakyan et al. (2022), we test if the same result can be obtained with our new prescribed wind model.

To perform this test, we ran additional simulations with a Saturn-mass planet $M_p = 0.3\ M_{Jup}$ and a disc with a thinner aspect ratio $h = 0.05$, a surface density power law of $p = 1$, and $\alpha = 10^{-3}$ instead of the usual constant viscosity. This α corresponds to $\nu = 2.5 \times 10^{-6}$ at the location of the planet. We focus on two wind strengths, our fiducial value of $b = 5 \times 10^{-4}$ and a weaker value of $b = 5 \times 10^{-5}$, but we also tested other wind strengths from $10^{-6} \leqslant b \leqslant 10^{-3}$. One set of simulations uses the K20 model including viscosity and the other set uses our new model. With no wind or low wind ($b \leqslant 5 \times 10^{-5}$) prescribed through either our model or the K20 model, the planet only triggers a weak elongated vortex that decays within 100 orbits after it formed. With a strong wind ($b \geqslant 5 \times 10^{-4}$) and the K20 model, however, the vortex is indeed stronger, as shown in the top left panel of Figure 17. It has a compact structure and shows little sign of decay after 1000 orbits.

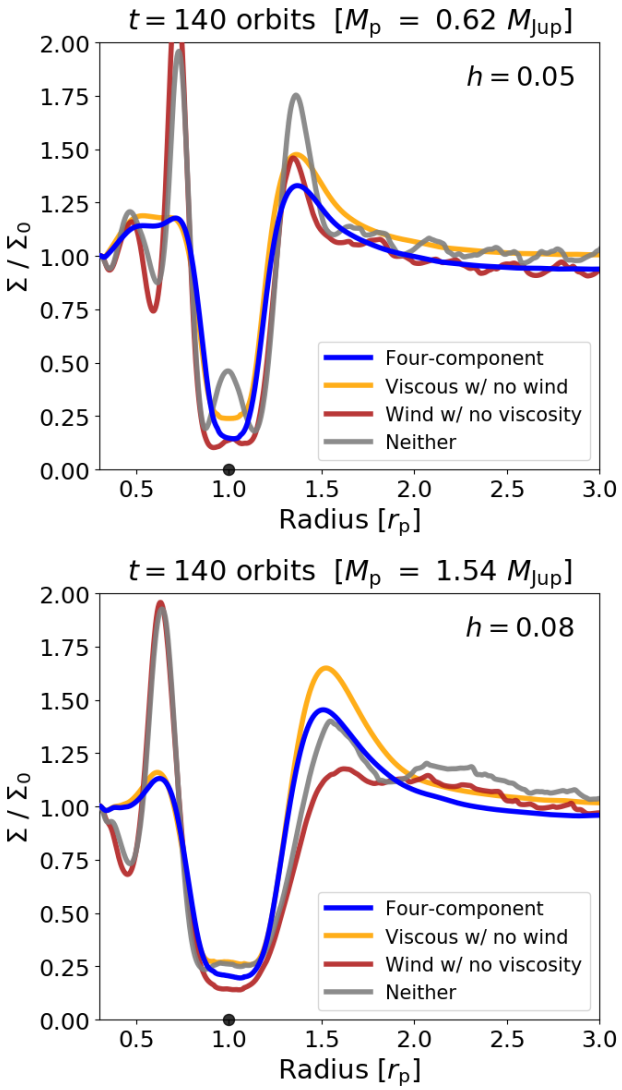

Figure 16. Low-aspect ratio comparison of the the full model (MHD-based torque, MHD-based mass loss, viscosity & extra gap torque) compared to just viscosity (*gold*), just wind (*red*), and neither (*grey*). The planet mass is 1 $M_{\rm Jup}$. Unlike at the fiducial aspect ratio of $h = 0.1$ from A&B 2023, viscosity does not elevate the pressure bump at the outer gap edge. At $h = 0.05$, the pressure bump drops with viscosity. At $h = 0.08$, the pressure bump is not significantly different until after $t = 140$. As a result, we are not optimistic viscosity would help produce a better fit, particularly at lower aspect ratios.

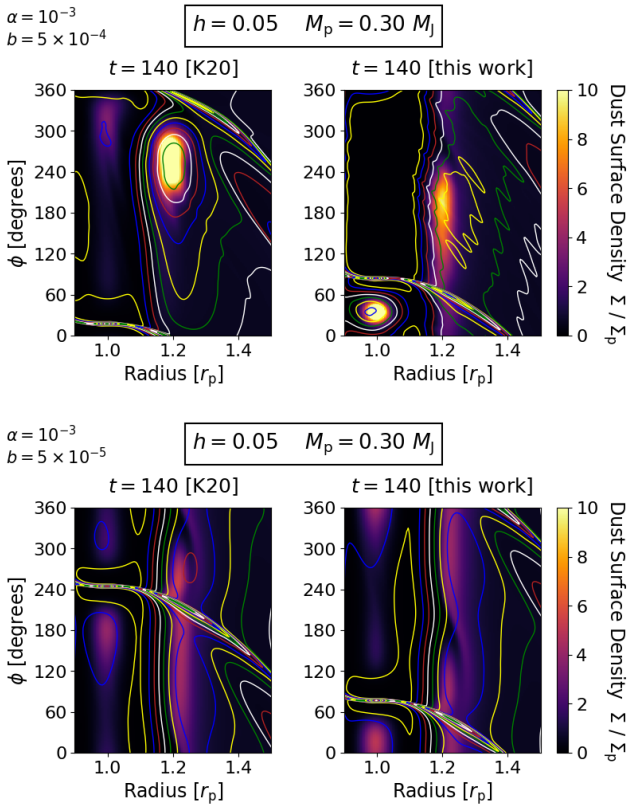

Figure 17. Dust density comparison for vortices with the prescribed wind models from K20 (K20: *left panels*) and this work (*right panels*). Gas density contours (at $\Sigma/\Sigma_{\rm p} = 0.4, 0.5, 0.6$, etc.) are overlaid. A strong wind (*top*) makes the vortex stronger with both models compared to a weaker wind (*bottom*), but the effect is much more pronounced with the K20 model.

With our new model, though, the vortex does not get stronger with stronger winds, as shown in the right panels of Figure 17. Regardless of the wind strength, it decays within 100 orbits. To determine how it can be so different, we compared the vortensity profiles, the criteria for triggering the RWI, with the different wind models. Although there were slight differences, we did not notice any obvious change that would indicate the other model would produce a stronger vortex.

4.3 Long-term evolution

One of the main drawbacks of MHD simulations of planets with disc winds thus far is the length of the simulations. Because of high computational expense, the simulations in A&B 2023 were only run for 140 planet orbits, which is insufficient to reach a steady state for the gap profiles. Other simulations by Wafflard-Fernandez & Lesur (2023) and Hu et al. (2025) were likewise only run for a few hundred orbits. As such, one of our main interests in developing a prescribed disc wind model was to enable simulations to run for thousands of orbits, enough time to reach more of a steady state.

We first tested running additional simulations with our fiducial parameters out to 3000 $T_{\rm p}$. Because the location of the outer gap edge continues to move outwards more than in our shorter simulations, we moved the outer edge of the domain further away from the planet from $r = 4$ to $r = 5.85$. We also increased the radial resolution from 768 cells to 1152 cells to keep the resolution the same. We tested two sets of cases, one set with our fiducial viscosity and one with no viscosity, and mainly varied the mass loss prescriptions. Each set consists of

(i) our full prescribed model,
(ii) our full model but with the simpler mass loss prescription from K20,
(iii) our full model but with no mass loss, and
(iv) a control case with no wind.

Every setup featured our fiducial 3 $M_{\rm Jup}$ planet and $h = 0.1$ disc, while the viscous cases all had $\nu = 10^{-5}$.

As Figure 18 shows, we find that the pressure bump moves much further away from the planet when there is a wind compared with no wind. The mass loss through the wind is a primary factor

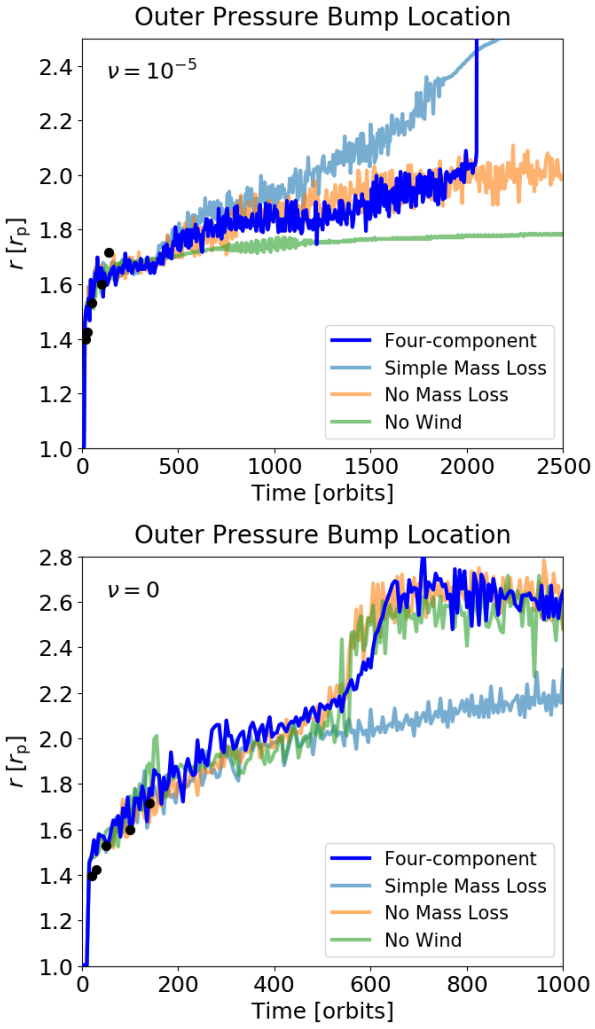

Figure 18. Pressure bump location with viscosity (*top*) and no viscosity (*bottom*) over time with different numbers of components to the prescribed wind. The values from A&B 2023 (*black dots*) at five different times are shown for comparison. In the viscous case, the wind causes the pressure bump to move further away from the planet, in part due to the mass loss depleting the bump. With no viscosity and the more realistic simple mass loss, the effect is the opposite, as the pressure bump is already further away from the planet.

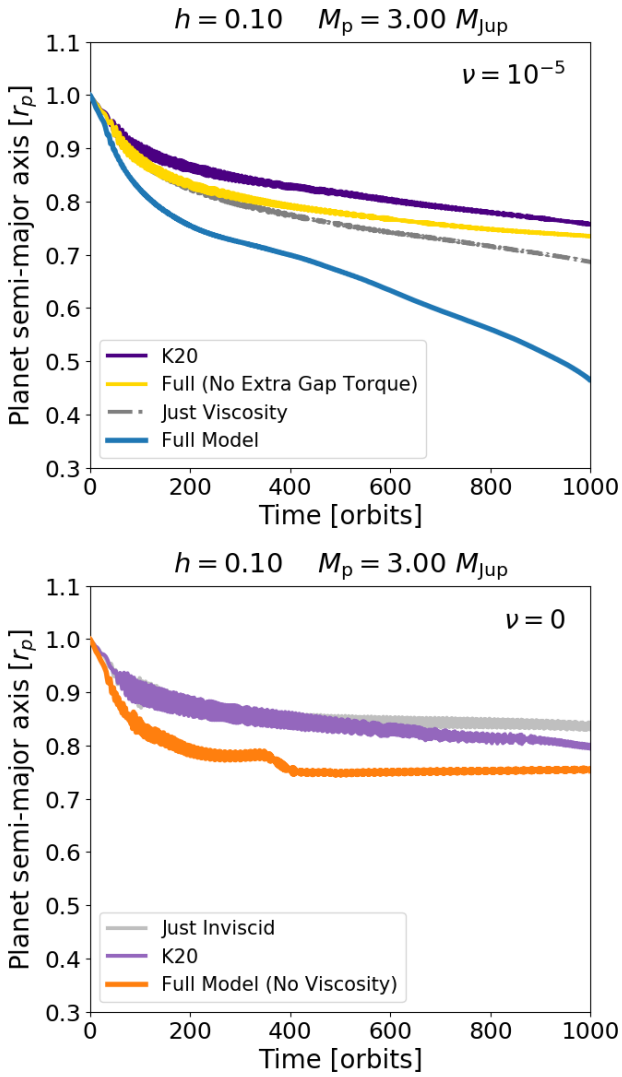

Figure 19. Planet migration tracks as a function of time with our fiducial parameters ($h = 0.1$, $\nu = 10^{-5}$, and $M_p = 3\ M_{Jup}$). Three main models are featured: [1] this work (*blue, orange, and yellow*), [2] the model from K20 (*purple and dark purple*), and [3] no wind (*grey and dark grey*). The variations leave out the viscosity or extra torque in the gap to illustrate their effects. The planet migrates inwards in all cases, and migrates the fastest with our full model from this work.

in moving the pressure bump away, which it does by depleting the bump when it starts out closer to the planet. It is not the only factor, though. Even with the lower-amplitude mass loss prescription from K20 or no mass loss at all, we see the pressure bump still ends up much further from the planet.

5 PLANET MIGRATION

Planet migration has thus far been the main application of prescribed wind models in 2D planet-disc interactions. One of the most atypical possibilities that has been found is the potential for disc winds to induce outward migration (K20). In order to test how disc winds affect planet migration with our model, we explore how the planet migrates both with our default parameters and in cases where outward migration has been found.

5.1 Fiducial migration

With our fiducial parameters, we find that our prescribed disc wind speeds up migration inwards compared to the K20 model or no wind. We tested two sets of cases, one set with our fiducial viscosity and one with no viscosity. Each set consists of

(i) our full prescribed model,
(ii) the K20 model
(iii) our full prescribed model but with no extra gap torque, and
(iv) a control case with just viscosity or no viscosity.

Every setup featured our fiducial 3 M_{Jup} planet and $h = 0.1$ disc, while the viscous cases all had $\nu = 10^{-5}$.

As Figure 19 shows, the planet migrates inwards in all cases regardless of the model or viscosity, but it migrates the fastest with our full model from this work. We see that the extra gap torque is the dominant factor in making the planet migrate faster, as we can

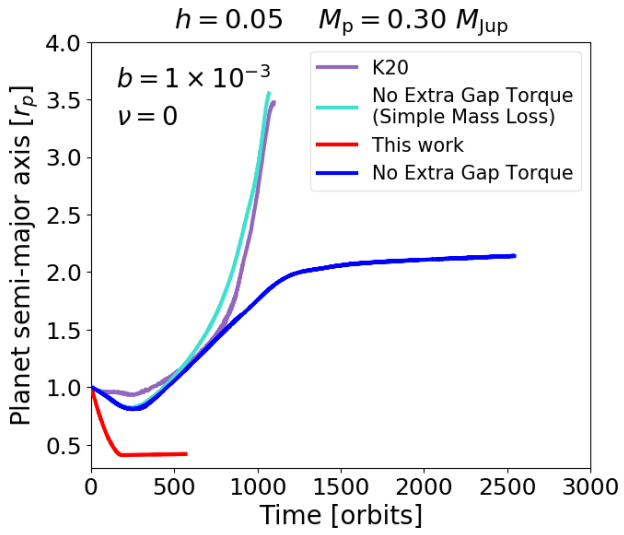

Figure 20. Planet migration tracks as a function of time, focusing on a case from K20 with outwards migration ($h = 0.1$, $M_p = 0.3\ M_{Jup}$, $b = 10^{-3}$, and $\nu = 0$). With the K20 model, the planet migrates runaway outwards after a few hundred orbits of slow inward migration. With our model, however, the planet migrates inwards rapidly due to the extra gap torque. Even without the extra gap torque, the planet migrates does not begin to migrate outwards until later, and the rate of outward migration is much slower.

tell from the control case where we removed it. Compared to the general control cases with no wind, the extra gap torque speeds up the migration both with and without viscosity.

5.2 Outward migration

To test if the planet can still migrate outwards with our model, we chose parameters from K20 that induced outwards migration. In particular, we lowered the surface density power law to $p = 0.5$ and set the disc aspect ratio to $h = 0.05$.

Our main set of runs has no viscosity and consists of

(i) our prescribed model,
(ii) the K20 model
(iii) our prescribed model but with no extra gap torque, and
(iv) our prescribed model but with no extra gap torque and the simpler mass loss prescription from K20.

We focused on Saturn-mass planets with $M_p = 0.3\ M_p$. With this low of a planet mass, K20 found the planet to migrate outwards with high wind strengths of $b > 4 \times 10^{-4}$. As such, we focus on a relatively high wind strength of $b = 10^{-3}$.

As Figure 20 shows, we observe the planet to migrate outwards using the K20 wind prescription, as did they. It initially migrates inward slowly before switching to a much faster outward migration. After a little over 1000 orbits, the planet reaches the outer boundary of the domain and then settles there only because that's the edge of the domain. With our model, however, the planet's initial inwards migration is much faster. Whereas the planet in the K20 disc never even reached $r = 0.95\ r_p$, the planet in the disc with our model reaches the inner boundary of the domain in a few hundred orbits. As a result, it does not even get the chance to reverse direction and migrate outward.

Like with our fiducial parameters, the rapid inward migration with our model is due to the extra gap torque. If we remove the extra gap torque, we see that the planet's inward migration slows down and it only reaches about $r = 0.7\ r_p$ before reversing direction outward. It then proceeds to runaway to the outer boundary like in K20.

Before the outwards runaway occurs, the planet migrates inwards more with our model than with theirs. Once the runaway begins though, the outward migration track ends up very similar, as long as the mass loss profile is the same. We note that the outwards migration tapers off much earlier with our fiducial mass loss profile, however, we believe that behavior is unrealistic because this mass loss profile is only intended for short-term simulations a few hundred orbits in length. This difference serves as an example reason to stick with the simple mass loss profile from K20 for long-term simulations.

We tested adding in viscosity and found that it does not have a significant effect on the migration tracks.

6 DISCUSSION

6.1 Validity of model

Beyond matching the MHD gap profiles with higher-mass planets, our best-fit model is physically motivated in several different ways. First, we use the radial torque profile from the MHD simulations, unlike existing prescribed disc wind models. Second, we have shown that the best fit for the gap profiles uses the exact level of torque inferred from MHD. Third, we incorporate a level of viscosity that is consistent with the MHD simulations, even if it is not possible to infer an exact value for the level of turbulence from the total Maxwell stress in MHD. And fourth, we have extra torque in the gap, as expected from the MHD simulations. These four aspects show our best-fit model is better physically motivated than other prescribed models regardless of how well it can fit the gap profiles.

The only component of our model that is less physically motivated is the mass loss radial dependence on the orbital frequency. We removed this dependence even though it appears the mass loss does scale with the orbital frequency from the MHD simulations. However, we stress that the purpose of removing the scaling isn't to match the background radial dependence. It is just to increase the mass loss near the gap edge. At the gap edge, the mass loss rate is higher in the MHD simulations compared to the rate we would have if we left in the scaling with orbital frequency that decays at larger radii. Removing the scaling was just the simplest way to increase the mass loss rate there. We also note the mass loss background profile does not have a strong impact on the gap profile in the gap or at the outer gap edge in short-term simulations of around a few hundred orbits. For these two reasons, we believe removing the scaling is physically motivated even if the purpose is not to get the right scaling. For long-term simulations, we recommend to use the simpler K20 mass loss prescription instead, as we have done in this study.

6.2 Applicability to simulations

We have demonstrated that our model works well for high-mass planets in discs with high aspect ratios with for a specific combination of wind strength and viscosity motivated by the simulations from A&B 2023.

Despite that success, we identified three main potential issues with the feasibility of using a prescribed wind model in place of

MHD. First, there is a narrow range of wind strengths and viscosities where both parameters affect the gap profile, instead of one dominating over the other. While it has some success in our model, it might not be practical to include both parameters if the ratio between the two were a bit more in favour of the wind or the viscosity. Second, adding in viscosity does not seem to help alter the gap profile in discs with lower aspect ratios in the same way it does at high aspect ratios. Third, with the presence of vortices at the gap edge, the problem of matching the MHD gap profiles reduces to some extent to matching the vortices from MHD.

Fortunately, none of these issues is necessarily a problem in general.

- With regard to the difficulties of combining wind strength and viscosity, it may actually be the case that only one of these parameters typically shapes the gap profile.
- With regard to the effects of viscosity being different at low aspect ratios, the viscosity was quite high in A&B 2023 mainly because they allowed MRI. If there were no MRI, viscosity may be less significant. If there were less viscosity, it may not actually affect planetary gap profiles in wind-driven discs or cause any issues, consistent with how our prescribed strong winds can dominate over prescribed weaker viscosities.
- Lastly, vortices may not be as much of an issue either. Although they dominate the gap profile early on, it is worth noting that with the high viscosity in our study, they disappear fairly quickly in only a few hundred orbits. After they are gone, matching the gap profiles goes back to being the simpler 1D problem. Even when they do appear, they may not be as difficult to match with lower planet masses or lower disc aspect ratios in discs with lower viscosity that are dominated by a wind.

Beyond those three issues, another issue to watch out for is the gas not depleting at the Lagrange point like in A&B 2023. It remains unclear though, whether the gas at the Lagrange point is supposed to deplete in MHD or not.

6.3 Applicability to observations

Disc winds may help to explain unusually wide planetary gaps. As one example, the asymmetric dust trap in Oph IRS 48, the first prominent dust trap ever identified, is unique in several ways (van der Marel et al. 2015). One oddity is that the asymmetry is located at 61 AU even though the gas cavity in the inner disc only extends to about 20 AU (van der Marel et al. 2013; Bruderer et al. 2014). If the asymmetry is indeed a vortex induced by a planet, this would suggest the planet is located about three times further in than the asymmetry, quite a large separation. In a viscous disc, such a large separation could be attained much more easily if there is also a disc wind present (with the simple mass loss prescription) compared to what would happen with no wind, as illustrated in Figure 18.

7 CONCLUSIONS

In this study, we test the efficacy of prescribed disc wind models in 2D planet-disc hydrodynamic simulations as a means to replicate or expand upon full 3D MHD disc wind simulations that are prohibitively expensive to run over a wide parameter space or for long simulation times.

By incorporating three main modifications based on the MHD simulations, we were able to reproduce the intermediate-stage gap profiles for planets with sufficiently high mass, but could not replicate the gap profiles for lower-mass planets. The three main changes we made to existing prescribed wind models were incorporating viscosity, adding extra torque in the gap, and flattening the torque radial profile. The viscosity helped match the gap profile at the outer gap edge and along the shoulder by elevating the amplitude of the pressure bump. The extra torque deepened the gap to better match the deeper gaps observed in MHD. The strength of the prescribed wind torque was taken from the MHD simulations, and the level of viscosity is also consistent with the MHD assuming only a small part of the Maxwell stress is turbulent.

One of the main caveats with our best gap profile fits is that they occur at a noticeable delay compared to the MHD, particularly for the gap depth. We observe that the hydrodynamic gap-opening process lags behind the MHD gap-opening process in general at all times, even at the very beginning. This lagging discrepancy lessens over time as the gap gets deeper. Much of the discrepancy comes directly from gas collecting at the co-orbital Lagrange point behind the planet, something that does not necessarily happen with MHD. We suspect the purely MHD-driven gap in the inner disc in MHD simulations, which is not created by the planet and was left out of our fiducial models, also indirectly helps deepen the gap. We find it surprising that the discrepancy occurs so early in the simulations before the gap has even opened, given that the extra torque in the gap mainly occurs due to the gap's reduced density.

With our model showing success for higher-mass planets, we attempted to extend it to longer simulation times and to other parameters, particularly thinner discs. At longer simulation times in viscous discs, we find that planets can open up much wider gaps in the presence of a wind, at least in terms of the location of the outer gap edge. For thinner discs, we note that viscosity is not needed to elevated the pressure bump, as it is already too strong with no viscosity. We caution that this trend also occurs with the low-mass planet gap profiles that we cannot fit. If, however, the shallow gap is the main reason we cannot fit the lower-mass gap profiles, we expect it may still be viable to use our prescribed model for thinner discs as long as the planet is massive enough to open a deep gap.

When we allow the planet to migrate, we observe that the extra torque in the gap drives faster inwards migration proportional to the wind strength. Adding in viscosity can also speed up migration, although not by as much as the extra gap torque. The fastest migration rates occur with both the extra gap torque and viscosity. In thinner-disc cases where runaway outward migration has previously been found, the extra gap torque provokes the planet to migrate inwards fast enough to avoid ever migrating outwards. On the other hand, viscosity does not stop outward migration, and can still allow runaway outwards migration.

One key to fitting the MHD gap profiles in general is to allow vortices, since these have been observed with MHD. This constraint limits the maximum viscosity that can be used in the model, since higher viscosities can weaken vortices or inhibit vortex formation altogether. It also makes it more difficult to fit the gap profiles in general since they are not truly 1D axisymmetric. Separately, we tested whether our prescribed model allows stronger long-lived vortices to form with high viscosities that would otherwise prevent them in wind-less discs. Even though such stronger vortices had been observed with existing prescribed models, we found that vortices in high-viscosities still remained weaker and shorter-lived with our model.

ACKNOWLEDGEMENTS

MH would like to thank Yuhiko Aoyama and Xuening Bai for helpful discussions about their study. MH would like to thank Leonardo Krapp for help with implementing the prescribed models in FARGO3D, and Lina Kimmig for helpful discussions about their study and also helping with the implementation. MH would like to thank Kees Dullemond, Richard Nelson, Sijme-Jan Paardekooper, and Paola Pinilla for hosting me to present this work, and the Dustbusters collaboration for organising the *New Heights in Planet Formation* conference where this work was presented. MH also would like to thank Amelia Cordwell, Can Cui, Thomas Rometsch, and Alex Ziampras for helpful discussions. Computations were performed on the kawas cluster at ASIAA. MH and MKL are supported by the National Science and Technology Council (grants 111-2112-M-001-062-, 112-2112-M-001-064-, 111-2124-M-002-013-, 112-2124-M-002-003-) and an Academia Sinica Career Development Award (AS-CDA110-M06).

DATA AVAILABILITY

The data underlying this article will be shared on reasonable request to the corresponding author.

REFERENCES

Alexander R., Pascucci I., Andrews S., Armitage P., Cieza L., 2014, in Beuther H., Klessen R. S., Dullemond C. P., Henning T., eds, Protostars and Planets VI The Dispersal of Protoplanetary Disks. p. 475
Andrews S. M., Huang J., Pérez L. M., Isella A., Dullemond C. P., Kurtovic N. T., Guzmán V. V., Carpenter J. M., Wilner D. J., Zhang S., Zhu Z., Birnstiel T., Bai X.-N., Benisty M., Hughes A. M., Öberg K. I., Ricci L., 2018, ApJ, 869, L41
Aoyama Y., Bai X.-N., 2023, ApJ, 946, 5
Bai X.-N., 2017, ApJ, 845, 75
Bai X.-N., Stone J. M., 2013, ApJ, 769, 76
Bai X.-N., Ye J., Goodman J., Yuan F., 2016, ApJ, 818, 152
Balbus S. A., Hawley J. F., 1998, Reviews of Modern Physics, 70, 1
Benítez-Llambay P., Krapp L., Pessah M. E., 2019, ApJS, 241, 25
Benítez-Llambay P., Masset F. S., 2016, ApJS, 223, 11
Blandford R. D., Payne D. G., 1982, MNRAS, 199, 883
Bruderer S., van der Marel N., van Dishoeck E. F., van Kempen T. A., 2014, A & A, 562, A26
Cui C., Bai X.-N., 2021, MNRAS, 507, 1106
de Val-Borro M., Artymowicz P., D'Angelo G., Peplinski A., 2007, A & A, 471, 1043
de Val-Borro M., Edgar R. G., Artymowicz P., Ciecielag P. e. a., 2006, MNRAS, 370, 529
Duffell P. C., 2015, ApJ, 807, L11
Elbakyan V., Wu Y., Nayakshin S., Rosotti G., 2022, MNRAS, 515, 3113
Ferreira J., Pelletier G., 1995, A & A, 295, 807
Fung J., Shi J.-M., Chiang E., 2014, ApJ, 782, 88
Hammer M., Kratter K. M., Lin M.-K., 2017, MNRAS, 466, 3533
Hammer M., Lin M.-K., 2023, MNRAS, 525, 123
Hammer M., Lin M.-K., Kratter K. M., Pinilla P., 2021, MNRAS, 504, 3963
Hartmann L., Herczeg G., Calvet N., 2016, ARA&A, 54, 135
Hu X., Li Z.-Y., Bae J., Zhu Z., 2025, MNRAS, 536, 1374
Kanagawa K. D., Muto T., Tanaka H., Tanigawa T., Takeuchi T., Tsukagoshi T., Momose M., 2015, ApJ, 806, L15
Kimmig C. N., Dullemond C. P., Kley W., 2020, A & A, 633, A4
Lega E., Morbidelli A., Nelson R. P., Ramos X. S., Crida A., Béthune W., Batygin K., 2022, A & A, 658, A32
Li H., Colgate S. A., Wendroff B., Liska R., 2001, ApJ, 551, 874
Li H., Finn J. M., Lovelace R. V. E., Colgate S. A., 2000, ApJ, 533, 1023
Li H., Li S., Koller J., Wendroff B. B., Liska R., Orban C. M., Liang E. P. T., Lin D. N. C., 2005, ApJ, 624, 1003
Lin M.-K., 2012, ApJ, 754, 21
Lovelace R. V. E., Li H., Colgate S. A., Nelson A. F., 1999, ApJ, 513, 805
Montesinos M., Garrido-Deutelmoser J., Olofsson J., Giuppone C. A., Cuadra J., Bayo A., Sucerquia M., Cuello N., 2020, A & A, 642, A224
Ono T., Muto T., Takeuchi T., Nomura H., 2016, ApJ, 823, 84
Riols A., Lesur G., Menard F., 2020, A & A, 639, A95
Shakura N. I., Sunyaev R. A., 1973, A & A, 24, 337
Surville C., Barge P., 2015, A & A, 579, A100
van der Marel N., Pinilla P., Tobin J., van Kempen T., Andrews S., Ricci L., Birnstiel T., 2015, ApJ, 810, L7
van der Marel N., van Dishoeck E. F., Bruderer S., Birnstiel T., Pinilla P., Dullemond C. P., van Kempen T. A., Schmalzl M., Brown J. M., Herczeg G. J., Mathews G. S., Geers V., 2013, Science, 340, 1199
Wafflard-Fernandez G., Lesur G., 2023, A & A, 677, A70
Wardle M., 2007, A&SS, 311, 35
Weidenschilling S. J., 1977, MNRAS, 180, 57
Wu Y., Chen Y.-X., Jiang H., Dong R., Macías E., Lin M.-K., Rosotti G. P., Elbakyan V., 2023, MNRAS, 523, 2630
Youdin A. N., Lithwick Y., 2007, Icarus, 192, 588